Journal of Geochemical Exploration 168 (2016) 103–118

Contents lists available at ScienceDirect

Journal of Geochemical Exploration

journal homepage: www.elsevier.com/locate/gexplo

Isotopic characteristics of gold deposits in the Yangshan Gold Belt, West Qinling, central China: Implications for fluid and metal sources and ore genesis

Li-Qiang Yang [a,*], Jun Deng [a,*], Nan Li [a], Chuang Zhang [a,b], Xing-Zhong Ji [a], Jin-Yuan Yu [a,c]

[a] State Key Laboratory of Geological Processes and Mineral Resources, China University of Geosciences, Beijing 100083, China
[b] Beijing Research Institute of Uranium Geology, Beijing 100029, China
[c] 12th Gold Mine Detachment of the Chinese Armed Police Force, Chengdu 610036, China

ARTICLE INFO

Article history:
Received 22 April 2015
Revised 24 May 2016
Accepted 13 June 2016
Available online 16 June 2016

Keywords:
Orogenic gold deposits
Yangshan gold belt
Stable isotopes
Metal source
Fluid evolution

ABSTRACT

The six main Triassic gold deposits of the Yangshan gold belt are hosted by Devonian metasedimentary rocks and Triassic granitic dikes. It has been suggested by previous workers that they are best classified as either Carlin-like or orogenic gold deposit types. Sulfide minerals spatially associated with disseminated and quartz vein-hosted gold mineralization at Yangshan were deposited in five stages that include syn-metamorphic, early ore, main ore, late ore, and post-ore stages. Based on the relationships defined by ore-mineral assemblages and paragenesis, H, O, C, S, Pb, and Sr isotopic data were obtained from sulfides, quartz, and ore host rocks. The $\delta^{18}O$ values of quartz from gold-bearing veins range from 15.9‰ to 21.5‰, and the calculated $\delta^{18}O_{H2O}$ values of ore-forming fluids vary from 6.4‰ to 11.8‰, which are consistent with those from typical orogenic gold deposits. The δD_{H2O} values of fluid-inclusions extracted from the quartz vary from −82‰ to −56‰, which are in accord with the δD_{H2O} values of most orogenic gold deposits. Interpretation of the $\delta^{13}C_{CO2}$ values (−4‰ to −2.5‰) in fluid inclusion, shows that marine carbonate is the dominant source for the carbon in the ore-forming fluids, with a minor contribution from magmatic sources. The $\delta^{34}S$ values of hydrothermal pyrite, arsenopyrite, and stibnite range from −6.6‰ to 3‰, which suggests sulfur is derived from a deep source. The Pb isotope values for hydrothermal sulfides from both the granitic dike-hosted ores and phyllite-hosted ores overlap the fields for their respective wall rocks, which suggests the source of lead is either the local host rocks, or ore-related fluids that may have pervasively penetrated the host rocks. The age-corrected $(^{87}Sr/^{86}Sr)_i$ values of pyrite are 0.70627 to 0.71304, and values for arsenopyrite are 0.71258 to 0.71294, showing that the strontium in the ore fluid could have been derived from the granitic dikes and the regionally extensive Mesoproterozoic to Neoproterozoic Bikou Group. The concordance of $\delta^{34}S$, Pb and $(^{87}Sr/^{86}Sr)_i$ values between those for hydrothermal sulfides and country rocks suggests that these crustal rocks contributed the gold that was subsequently concentrated in the ore deposits. The syn-metamorphic stage and early ore stage fluids were likely derived from the country rocks during prograde metamorphism at depth. The oxygen isotope compositions indicate relatively widespread interaction of such fluids with $\delta^{18}O$-rich country rocks during the main ore stage. Compared with most orogenic gold deposits and Carlin-type gold deposits, the gold deposits in the Yangshan gold belt exhibit isotopic characteristics that are most like those of orogenic gold deposits.

1. Introduction

Although many of the ore forming characteristics of orogenic gold deposits are reasonably well understood, debate continues on their genesis largely because it is difficult to reliably identify the source of the gold (Goldfarb et al., 2005, 2014; Phillips and Powell, 2009; Large et al., 2011; Tomkins, 2013). Isotopic data (e.g. C, H, O and S) from orogenic gold deposits can indicate a variety of possible sources for ore fluids and metals (Goldfarb and Groves, 2015). Most isotopic tracers are not diagnostic of a fluid or metal source because of the isotopic exchange between ore fluids and wall rocks, uncertainties in degree of isotopic fractionation during ore mineral precipitation, and possible post-ore resetting of isotopic settings (McCuaig and Kerrich, 1998; Ridley and Diamond, 2000; Groves et al., 2003). Isotopic research based on spatial and temporal variation between mineral grains may shed light on the metal sources and ore-forming fluid evolution (Chen et al., 2012; Deng et al., 2011, 2014a).

* Corresponding authors at: State Key Laboratory of Geological Processes and Mineral Resources, China University of Geosciences, 29# Xue-Yuan Road, Haidian District, Beijing 100083, China.
E-mail addresses: lqyang@cugb.edu.cn (L.-Q. Yang), djun@cugb.edu.cn (J. Deng).

http://dx.doi.org/10.1016/j.gexplo.2016.06.006
0375-6742/

Table 1
Characteristics of the main orebodies in the Yangshan gold belt.

Gold deposit	Orebody assemblage number	Gold reserves (kg)	Gold grade (g/t) (average)	Thickness of orebody (m) (average)	Inclination of orebody	Wall rock	Mineralization pattern
Anba	305	94,390	5.35	4.84	150–175° ∠ 45–70° 320–340° ∠ 45–60° 150–175° ∠ 45–70° 320–340° ∠ 45–60°	Altered phyllite, granite	Disseminated
	360	68,038	4.40	4.71	160–170° ∠ 48–68° 160–170° ∠ 48–68°	Altered phyllite, granite	Disseminated
	311	104,936	4.69	3.35	150–175° ∠ 55–65° 150–175° ∠ 55–65°	Altered phyllite, granite, quartz veins (locally)	Veinlet, disseminated
Yangshan	2	11,527	9.62	2.78	20–40° ∠ 20–36° 20–40° ∠ 20–36°	Altered granite, cataclastic limestone	Blocky, veinlet, disseminated
	13	6486	3.13	7.02	185–205° ∠ 42–60° 185–205° ∠ 42–60°	Altered phyllite, granite, limestone	Blocky, veinlet, disseminated
Getiaowan	402	6923	4.63	3.24	330–20° ∠ 30–45° 330–20° ∠ 30–45°	Altered phyllite, granite	Disseminated
	403	811	4.71	4.53	165–205° ∠ 53–70° 165–205° ∠ 53–70°	Altered phyllite, granite	Disseminated
	404	866	2.12	2.19	330–10° ∠ 20–45° 330–10° ∠ 20–45°	Altered phyllite, granite	Disseminated
Nishan	501	/	2.22	3.18	160–200° ∠ 45–75° 160–200° ∠ 45–75°	Altered granite	Disseminated
	504	/	5.80	1.09	340–10° ∠ 60–85° 340–10° ∠ 60–85°	Altered phyllite, granite	Disseminated
	506	/	4.15	3.07	5–45° ∠ 45–70° 5–45° ∠ 45–70°	Cataclastic phyllite, granite	Veinlet, disseminated
	508	/	1.58	4.63	160–190° ∠ 40–60° 160–190° ∠ 40–60°	Altered phyllite, granite	Disseminated
	509	/	1.67	2.37	170–10° ∠ 45–65° 170–10° ∠ 45–65°	Altered phyllite, granite	Disseminated
Zhangjiashan	101	/	0.03–1.18	1.40	330–350° ∠ 50° 330–350° ∠ 50°	Altered granite, silicified phyllite	Disseminated
	102	/	2.27, 0.52	7.76–28.44	355° ∠ 40°	Altered granite, cataclastic phyllite with limestone	Veinlet, disseminated
Gaoloushan	201	/	0.5–12.8	0.5–2	185–210° ∠ 30–55°	Altered phyllite	Disseminated
	207	/	4.06	3.56	200–260° ∠ 35°	Altered phyllite	Disseminated
	209	/	2.46	2.47	200–230° ∠ 25–45°	Altered phyllite	Disseminated

Table 1 (*continued*)

Gold deposit	Orebody assemblage number	Gold reserves (kg)	Gold grade (g/t) (average)	Thickness of orebody (m) (average)	Inclination of orebody	Wall rock	Mineralization pattern
	210	/	3.60	4.00	84–101° ∠ 36–46°	Altered phyllite	Disseminated

The Yangshan gold belt contains a series of gold deposits in central China with a very large gold resource (>350 t Au) (Yan et al., 2010), and mining is scheduled to begin in 2016. However, there is debate concerning the genesis of the gold in the Yangshan gold belt, as to whether these gold deposits are Carlin-like type (Li et al., 2008; Zhang et al., 2009; Lei, 2011) or orogenic type (Li et al., 2014). The gold belt is located in the Mian–Lue Suture Zone in the West Qinling Orogenic Belt and formed during post-collisional tectonism of the North China Block and Yangtze Craton (Dong et al., 2011; Yang et al., 2015a,b). Although the Anba gold deposit hosts >90% of the gold resources in the belt, all the deposits have similar geological and mineralogical characteristics (Table 1). The gold orebodies in the gold belt are hosted in Devonian phyllite, marble and metasandstone, and acidic magmatic dikes, or along the contact belt between the dikes and phyllite (Table 1). The major part of the gold ore is disseminated in the host rocks with minor amounts occurring in pyrite–arsenopyrite quartz veins, stibnite-bearing quartz veinlets, and quartz–calcite veins (Table 1; Li et al., 2014). Previous researchers (Luo et al., 2004; Wen, 2006; Yang et al., 2007; Li et al., 2008; Zhang et al., 2009) have presented isotopic data for the gold deposits in the Yangshan gold belt. However, the interpretation of these isotope data is constrained by the lack of stated relationships to the complex paragenesis of the examined minerals. For example, the samples collected for H and O isotope analyses by Luo et al. (2004) are from a pyrite–quartz vein whose paragenetic stage is not stated. Li et al. (2008) examined C, H, and O stable isotopes for samples from the Anba and Getiaowan gold deposits, but the lack of petrological evidence for the different stages of quartz and the limited number of samples from only two gold deposits limit the significance of the data. Zhang et al. (2009) used Sr and Pb isotopes to trace the source of the ore fluids and metals. However, the interpretation of these radiogenic isotope data is limited by the lack of information on the relative ages of the different ore stages. Furthermore, the study corrected the Sr and Pb isotopic measurements using an age of 190 Ma, which is not the age of the gold deposits. Sulfur isotope studies indicate a number of different sulfur sources (Luo et al., 2004; Yang, 2006; Li et al., 2012), suggesting that there are problems in using a single isotope system to reveal a fluid source reservoir.

In this paper, we describe the geological setting and lithology of the Yangshan gold belt and present results of isotopic geochemistry from sulfides, quartz from different ore stages, and various host rocks, along with a comparison of isotopic characteristics of other orogenic gold systems and Carlin-type gold deposits. The paper is thus aimed at augmenting the existing knowledge of the isotopic geochemistry of gold deposits in general, using the Yangshan gold belt as an example. The source of the fluids and metals, and the origin of the deposit, are discussed through the detailed isotope studies (H–O–C–S–Pb–Sr) in the Yangshan gold belt, thereby improving our understanding of gold mineralization and in turn exploration success along the Mianlue Suture Zone, West Qinling, central China.

2. Regional and local geology

The Qinling Orogenic Belt in central China is a collisional orogen that is >1500 km long and ~200–250 km wide, and separates the North China and South China Blocks (Fig. 1; Mattauer et al., 1985; Zhang et al., 1995, 2001; Meng and Zhang, 1999, 2000; Dong et al., 2014). It can be divided into the North and South Qinling Blocks. The North Qinling Block is separated from the North China Block by the Erlangping Suture Zone, and from the South Qinling Block by the Shangdan Suture Zone (Zhang et al., 1995; Sun et al., 2000). The South Qinling Block in the southernmost part of the orogenic belt is separated from the South China Block by the Mianlue Suture (Zhang et al., 1995; Meng and Zhang, 1999, 2000; Xu et al., 2002). These three suture zones, marked by various ophiolite complexes and mélange units separating subduction–accretion systems, display a complex record of discrete ocean basin evolution within the broader Paleotethyan realm (Yang et al., 2015b).

The tectonic evolution of the Mianlue Suture includes a rifting event in the Devonian, followed by subduction during the Late Permian, and continent–continent collision in the Middle–Late Triassic (Zhang et al., 2004). The suture extends W–E to WNW–ESE (Fig. 1), with its eastern part being cut by the southern domain of the Dabie orogen; it extends to the Wenxian and Derni areas, and further west to the southern part of the Dabashan, Mianxian, Lueyang and Kangxian areas, and connects with the Eastern Kunlun orogen in the west (Zhang et al., 2004). A series of south-verging large-scale arc-shaped thrust nappe structures has been identified in the Mianlue Suture (Zhang et al., 2004). Among these, the southern edge of the Dabie–Tongbai, Dabashan, and the Kangxian–Wenxian–Nanping Arcs are the three major thrust nappe structures identified (Fig. 1).

The Yangshan gold belt is structurally controlled by the Wenxian arcuate structure which lies at the southern tip of the Kangxian–Wenxian–Nanping Arc (Zhang et al., 1996; Du and Wu, 1998; Pei et al., 2002; Deng et al., 2014b). The structure comprises three E–W-trending faults, the Songbai–Liping, Majiamo–Weijiaba, and Baima–Linjiang Faults, with overprinting N–S-trending faults (Du and Wu, 1998; Yan et al., 2010). The 30 km long E–W-striking Anchanghe–Guanyinba Fault is a branch of the Songbai–Liping Fault, with a width varying from tens to thousands of meters. The fault mainly dips to the north and the dip angle changes from 50° to 70°, which is commonly parallel to the foliation of the phyllitic country rocks. The Anchanghe–Guanyinba Fault has three secondary faults, termed F1, F2, and F3 (Fig. 2). The major fold in the gold belt is the E–W-striking Getiaowan–Caopingliang Anticline, which extends for about 10 km, with a width of 1 km. The orebodies of the Yangshan gold belt are controlled by the Anchanghe–Guanyinba Fault system and the Getiaowan–Caopingliang Anticline and a series of secondary ENE-trending faults (Li et al., 2014). The Anchanghe–Guanyinba Fault system cuts the Wujiashan Syncline, which is the largest syncline in the gold belt.

The Yangshan gold belt is 30 km long and includes six gold deposits (from west to east) Nishan, Getiaowan, Anba, Gaoloushan, Guanyinba and Zhangjiashan (Fig. 2). They were formed at about 208 Ma based upon ^{40}Ar–^{39}Ar dating of hydrothermal sericite (Li, 2013a). The Bikou Group is the oldest unit in the region, and makes up the northern margin of the Yangtze Craton and the southern margin of the gold belt. It consists of Mesoproterozoic to Neoproterozoic metamorphosed volcanic–sedimentary rocks (Yan et al., 2003, 2010). The Devonian Sanhekou Group is the main host for the deposits of the Yangshan gold belt. These rocks comprise a very thick unit of shallow-water clastic and carbonate-rich sedimentary formations consisting of greenschist facies phyllite, slate, marble, and sandstone (Yang et al., 2015b).

There are no large igneous intrusions in the gold belt. Small intrusive bodies, termed the Puziba granitoids, comprise granite, aplite, and porphyry dikes. The Puziba dikes were sheared into lenses along the E–W-trending Anchanghe–Guanyinba Fault system (Yang et al., 2015b). Quartz, sericite, carbonate, sulfide, chlorite, epidote, illite, and kaolinite

alteration minerals are common in the dikes in the gold belt (Yan et al., 2010). Zircon U–Pb dating of unaltered granitic dikes indicates that they were emplaced at ca. 210 Ma (Qi et al., 2005; Yang et al., 2006; Lei, 2011). In terms of composition and emplacement age, the Puziba dikes are similar to larger stocks and plutons located on the southern edge of the South Qinling Block to the north and the Bikou Block to the south of the Mianlue Suture Zone (Sun et al., 2002; Qin et al., 2008).

3. Gold mineralization styles and stages

Gold-bearing pyrite, arsenopyrite, and stibnite are disseminated in phyllite (Fig. 3a), granitic dikes (Fig. 3b), marble (Fig. 3c), and graywacke. Less commonly sulfides occur in small veins or veinlets that cut these host rocks (Fig. 3d), although for paragenetic studies, the veins provide the more important samples that can define mineral assemblages developed during each stage. Phyllite and granitic dikes are the major host rocks for the disseminated ores in all six gold deposits, although marble, with a limestone protolith, is also important at the Guanyinba gold deposit. Phyllite is grey in color, with lepidoblastic texture and phyllitic structure and it is mainly composed of fine-grained quartz, sericite, kaolinite, and illite, with minor amounts of chlorite, epidote, and calcite. The dikes are granitic in composition, with microgranular and (or) porphyritic textures. They consist of phenocrysts of K-feldspar, plagioclase, quartz, and minor biotite, and accessory magnetite, zircon, and apatite. The matrix is mainly composed of oligoclase, K-feldspar, quartz, and biotite. The grey marble has a cryptocrystalline texture and massive structure, and is composed of calcite, sericite, chlorite, and commonly cross-cut by calcite–quartz veins. The graywacke is pink or grey in color, with palimpsest texture and massive structure, and it is composed of quartz, mica, and minor chlorite, epidote, and hematite. The mineralized quartz veins occur along the contact between phyllite and granitic dikes, or within granitic dikes (Fig. 3d).

Based on the cross-cutting relationship among different veins, and the features of minerals in different ore stages as clearly defined by Li et al. (2014), five paragenetic sulfide stages in the Yangshan gold belt were defined. Syn-metamorphic pyrite (Py_0) has a framboidal or colloform texture and is disseminated in the metasedimentary host rocks (Fig. 3e) or in syn-metamorphic quartz veins. The syn-metamorphic quartz veins are narrow (<2 cm wide) and straight, with sparse pyrite grains, as well as calcite and illite that has been locally transformed into sericite and replaced by chlorite during progressive metamorphism. Hydrothermal pyrite (Py_1) in the early ore stage is present in quartz veins, but mainly is disseminated in metasedimentary rocks and dikes, and also present as aggregates or bands in phyllite. The early ore stage quartz veins experienced strong tectonic deformation, are curved in shape, and are defined by a pyrite–quartz–sericite association (Fig. 4c, d; Supplementary table 1). The main ore stage pyrite (Py_2), commonly overgrows Py_1 and is typically associated coeval arsenopyrite (Apy_2) (Fig. 3f). Quartz veins formed during this stage have been sheared into an "S" shape and show an arsenopyrite–pyrite–quartz–sericite assemblage (Fig. 4e, f; Supplementary table 1). Late ore stage pyrite (Py_3), arsenopyrite (Apy_3), and stibnite occur in quartz ± calcite veins or are disseminated in country rocks, and overprint the main ore stage sulfides (Fig. 3g). The late ore stage quartz ± calcite veins are extensional and sheared, locally showing comb texture, with an association of stibnite–gold–arsenopyrite–pyrite–quartz–calcite–kaolinite–sericite (Fig. 4g, h; Supplementary table 1). Gold is mostly present as "invisible gold" within pyrite and arsenopyrite in the three ore-bearing stages, although some native gold, irregular in shape, also

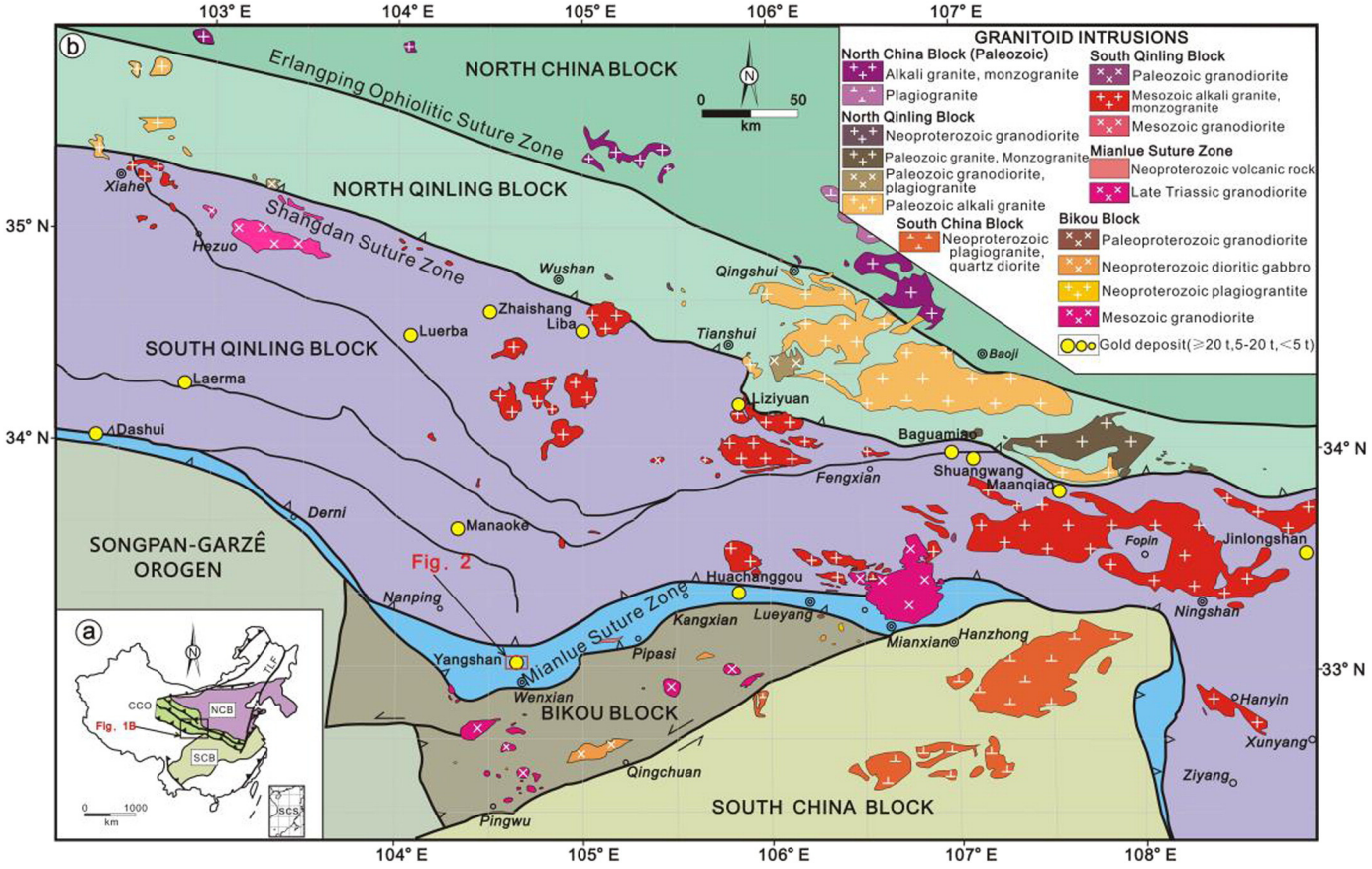

Fig. 1. Simplified regional geologic map of Western Qinling, showing the location of major Au deposits. (a) Simplified tectonic map of China showing the location of the research area and related cratonic blocks, orogenic belts, and major faults (modified from Zhao et al., 2001). NCB, North China Block; SCB, South China Block; CCO, Central China Orogen. (b) Simplified regional geologic map of Western Qinling, showing the location of major Au deposits (modified from Dong et al., 2011 and Yang et al., 2015a).

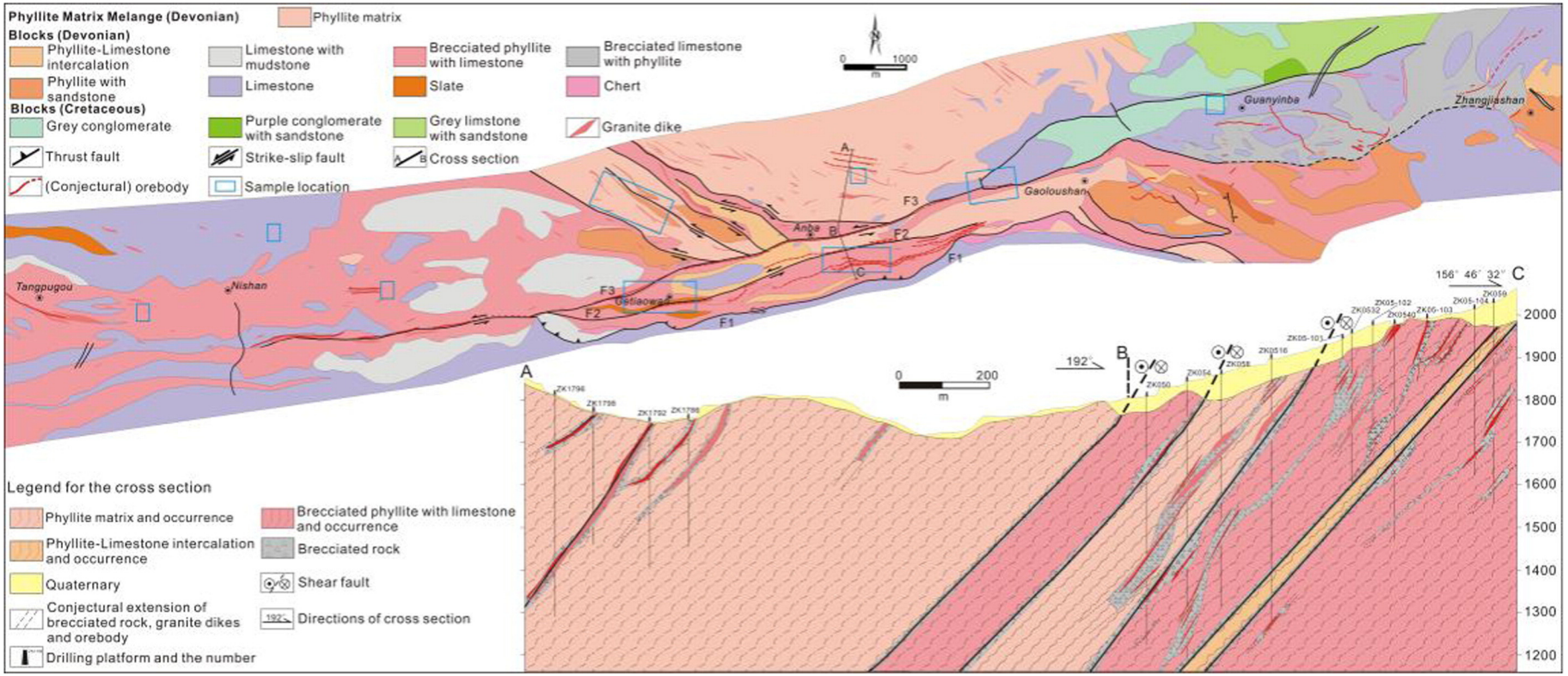

Fig. 2. Simplified geological map of the Yangshan gold belt (see Fig. 1b for location).

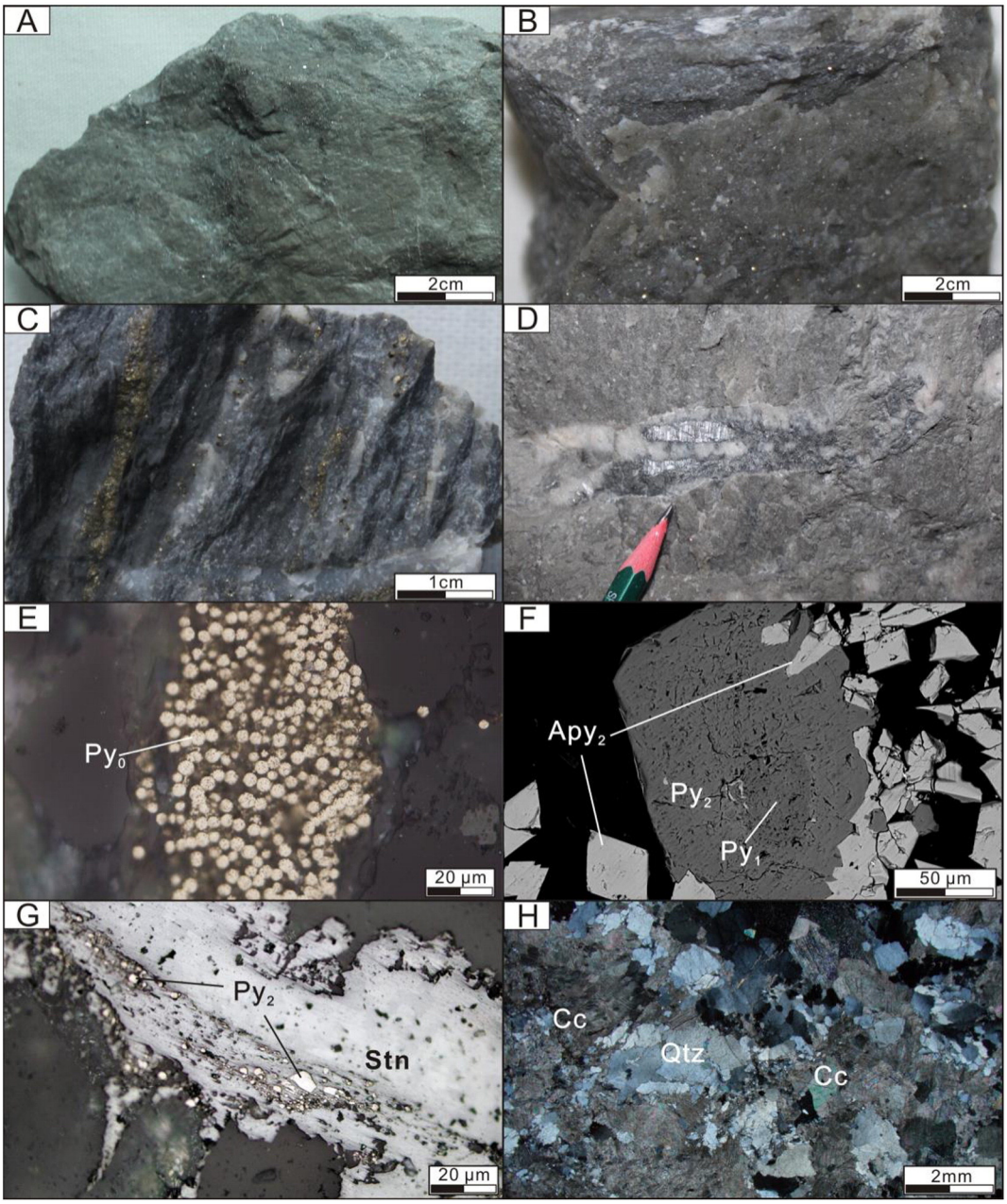

Fig. 3. Ore textures and paragenetic stages of the gold deposits in the Yangshan gold belt. (a, b, c) Disseminated pyrite and arsenopyrite in phyllite, granitic dikes, and marble, respectively. (d) Stibnite occurs in quartz veins that cut granitic dikes (pencil for scale). (e) Framboidal pyrite in the metasedimentary host rocks. (f) Main ore-stage pyrite (Py_2) commonly overgrows Py_1, and Py_2 is associated with main ore-stage arsenopyrite (Apy_2). (g) Main ore-stage pyrite (Py_2) is overprinted by late ore-stage stibnite in quartz ± calcite veins. (h) Late ore-stage quartz–calcite vein.

occurs in the late ore stage (Li et al., 2014). Post-ore stage pyrite (Py_4) occurs in quartz ± calcite veins (Fig. 3h) that cut all earlier mineralization (Supplementary table 1; Fig. 6 in Li et al., 2014). In addition to the above minerals, there are minor amounts of other sulfides (chalcopyrite, galena, and sphalerite), as well as sulfosalts (boulangerite, jamesonite, famatinite, tennantite, and bournonite) in the early, main, and late ore stages (Li et al., 2014). Oxidized gold ores are characterized by high limonite and magnetite contents and occur near the surface (Qi et al., 2003).

4. Sampling and analytical methods

Sixty-nine representative samples were collected from outcrops and underground workings in the Nishan, Getiaowan, Anba, Gaoloushan, and Guanyinba gold deposits. Samples were crushed to between 40 and 80 mesh for mineral separation. Pyrite, arsenopyrite, stibnite, and quartz were handpicked under a binocular microscope. The purity of a single mineral separate was >99%. All mineral separates were cleaned in an ultrasonic bath before being powdered in an agate mortar. Quartz separates were analyzed for O isotopes, bulk fluid-inclusion waters extracted from the quartz were analyzed for C and H isotopes, and sulfide mineral separates were analyzed for S and Pb isotopes.

Hydrogen and carbon isotopic compositions of fluid inclusions in quartz and oxygen isotopic values in quartz were analyzed in the Stable Isotope Laboratory of the Institute of Mineral Resources, Chinese Academy of Geological Sciences, Beijing, using a Finnigan MAT253 mass spectrometer. Oxygen was liberated from quartz for isotopic analyses by reaction with BrF_5 (Clayton et al., 1972), and converted to CO_2 on a platinum-coated carbon rod. For analysis of hydrogen isotopes, water

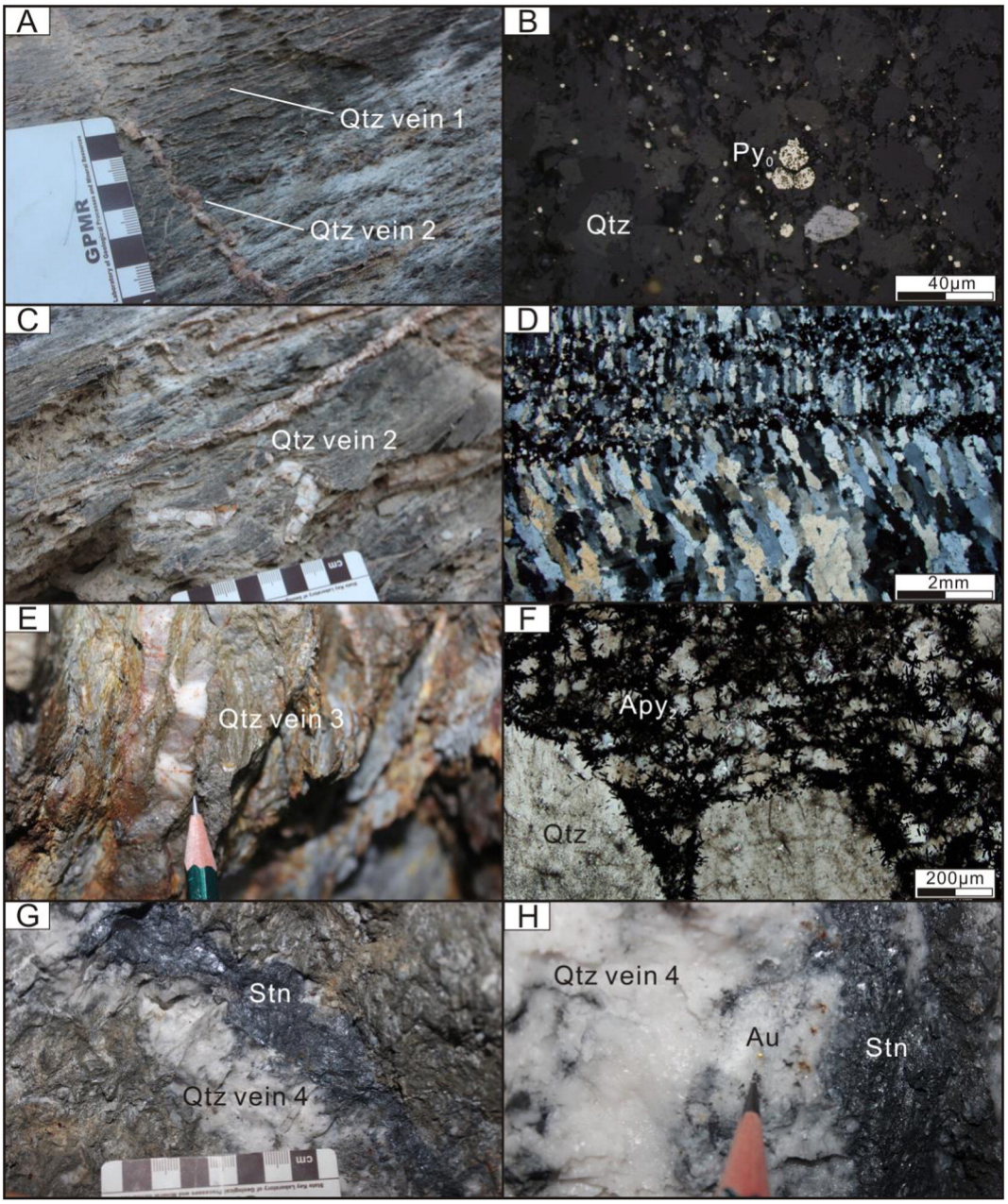

Fig. 4. Geological characteristics of quartz veins in the Yangshan gold belt. (a) Early ore-stage quartz vein (Qtz vein 1) cuts syn-metamorphic stage quartz veins (Qtz vein 2). (b) Syn-metamorphic framboidal pyrite (Py_0) is disseminated in syn-metamorphic quartz (Qz) veins. (c) Highly deformed early ore-stage quartz vein (Qtz vein 2). (d) Quartz grains in the early ore-stage quartz vein (Qtz vein 2) that are recrystalized and elongated. (e) White-smoky-grey main ore-stage lenticular quartz vein (Qtz vein 3) with pyrite and arsenopyrite. (f) Massive arsenopyrite (Apy) in the main ore-stage quartz veins (Qtz vein 3). (g) Extension and sheared late ore-stage quartz veins (Qtz vein 4), of variable width, mainly composed of quartz and stibnite (Stn). (h) Native gold grains (Au) disseminated in late ore-stage quartz veins (Qtz vein 4). Centimeter scale in (a, c, g); pencil for scale in (e, h).

from fluid inclusions was released from the quartz samples by heating to ~600 °C, which reacted with zinc to produce hydrogen at 410 °C. For carbon isotope analysis, gas was generated by heating the quartz and the CO_2 from the released gas was collected, and then frozen and purified in a nitrogen and alcohol cooling trap. The H and O data are reported using Standard Mean Ocean Water (V-SMOW) and the C data using the Pee Dee Belemnite (V-PDB) as standards, with a precision of ±2‰ for δD and ±0.2‰ for $\delta^{18}O$ and $\delta^{13}C$.

Sulfur isotopes were analyzed at the US Geological Survey laboratories in Denver (USA). Pure mineral samples were weighed with V_2O_5, then combusted and analyzed for ^{34}S according to method of Giesemann et al. (1994) using a Costech Analytical Elemental Analyzer coupled to a Thermo Finnigan Delta Plus XL mass spectrometer. Sulfur isotope compositions are reported relative to Cañon Diablo Troilite (CDT) with a precision of 0.2‰.

Powdered whole-rock samples were analyzed for Pb and Sr isotopes. The Pb isotope analyses were carried out in the Isotope Laboratory of the Institute of Geology, Chinese Academy of Geological Sciences. The Pb isotope ratios were measured with a Thermo Finnigan Triton thermal ionization mass spectrometer by a Nu Plasma HR instrument MC-ICP-MS, and the mass fractionation of the instrument was corrected by an external standard of Tl isotopes (He et al., 2005) in which lead and half of the Tl were mixed into the sample. The sulfide samples for Pb isotope analysis were dissolved in HNO_3 and HCl, and the whole-rock samples were dissolved in HF + HNO_3, passed through an anion exchange resin for Pb extraction, and diluted by 1% HNO_3 for testing after drying

of the solution. Lead isotope data are provided after normalization to the accepted ratio for NBS-981: $^{208}Pb/^{206}Pb = 2.16736 \pm 0.00066$, $^{207}Pb/^{206}Pb = 0.91488 \pm 0.00028$, $^{206}Pb/^{204}Pb = 16.9386 \pm 0.0131$, $^{207}Pb/^{204}Pb = 15.4968 \pm 0.0107$, $^{208}Pb/^{204}Pb = 36.7119 \pm 0.0331$ ($\pm 2\sigma$).

The Sr isotope analyses were carried out in the Isotope Laboratory of the Institute of Geology, Chinese Academy of Geological Sciences. The sample powders for Sr isotope analysis from fresh granitoid dikes were ground to minus-200 mesh and dissolved on a hot plate with 2 mL 6 M HNO_3 and 10 mL 23 M HF. The initial chemical separation of Sr followed standard ion exchange procedures: the solution was loaded into a quartz column packed with AG50W × 8(H^+), (200–400 mesh) ion exchange resins. The REE fraction was further separated on a 2 mL column of Teflon powder coated with di-2-ethylhexyl phosphoric acid. The Sr isotope ratios were measured on a Finnigan MAT 262 thermal ionization mass spectrometer equipped with a multi-collector. During the analytical period, several measurements of NIST SRM 987 (formerly NBS 987) Sr reference samples gave the following values: $^{87}Sr/^{86}Sr = 0.710232 \pm 15$ (2SE); mass fractionations were corrected to $^{88}Sr/^{86}Sr = 8.37521$ and total procedural blanks were about 10^{-9} to 10^{-10} g Sr. The $(^{87}Sr/^{86}Sr)_i$ values of sulfides and whole rocks are age-corrected using the ore-formation age of 208 Ma (Li, 2013a).

5. Analytical results

5.1. $\delta^{18}O$, δD, and $\delta^{13}C$ composition of quartz and fluids

The $\delta^{18}O$ values of syn-metamorphic and hydrothermal quartz range from 15.9 to 21.5‰ (Table 2). The $\delta^{18}O$ value of syn-metamorphic stage quartz is 18.5‰. The $\delta^{18}O$ values of early, main and late ore stage quartz range from 15.9 to 17.0‰, 17.6 to 21.5‰, and 18.4 to 21.1‰, respectively.

Based on the mineral paragenesis observations and homogenization temperatures for the primary aqueous and aqueous–carbonic fluid inclusions in quartz (300 °C for the syn-metamorphic stage; 295 °C, 235 °C, and 195 °C for the early, main, and late ore stages, respectively: Li et al., 2007), the ranges and average values for calculated $\delta^{18}O_{H2O}$ of syn-metamorphic and ore-related quartz are shown in Table 2. The calculated $\delta^{18}O_{H2O}$ value of syn-metamorphic quartz is 11.6‰. The calculated $\delta^{18}O_{H2O}$ values of early, main, and late ore stage quartz are 8.8–9.9‰, 7.9–11.8‰, and 6.4–9.1‰, respectively.

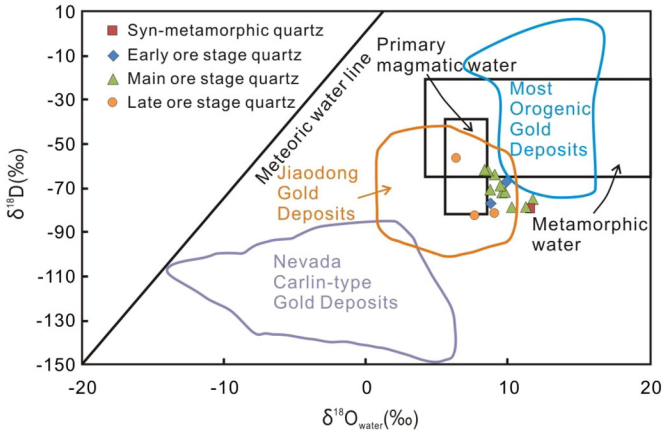

Fig. 5. The δD_{H2O} values of fluid inclusions and calculated $\delta^{18}O_{H2O}$ values at Yangshan. References for the fields of other deposits are given in the text.
Fields for magmatic and metamorphic waters are from Taylor (1987).

The δD_{H2O} values of fluid inclusions released from syn-metamorphic and ore-related quartz range from −82 to −56‰ (Table 2). The δD value of syn-metamorphic quartz is −79‰. The δD values for early, main, and late ore stage quartz samples range from −77 to −67‰, −78 to −61‰, and −82 to −56‰, respectively (Fig. 5). The $\delta^{13}C_{CO2}$ values in fluid inclusion for syn-metamorphic quartz is −4.0‰ and for early, main, and late ore stages are −3.8‰, −3.9 to −2.5‰, and −3.6 to −3.3‰, respectively (Table 2; Fig. 6).

5.2. $\delta^{34}S$ and Pb isotope composition of sulfides and fluids

The pyrite from syn-metamorphic veins in phyllite has $\delta^{34}S$ values ranging from −29‰ to +24.6‰, and from marble the values range from 15.3‰ to 17.5‰ (Fig. 7; Luo et al., 2004; Yang, 2006; Yan et al., 2010). The $\delta^{34}S$ values of hydrothermal pyrite from the gold deposits of the Yangshan gold belt have a narrow range of −2.1‰ to +1.2‰, (Table 3; Fig. 7). The $\delta^{34}S$ values of main ore-stage arsenopyrite range from −4.2‰ to +3.0‰ and the $\delta^{34}S$ values of stibnite range from −6.6‰ to −4.5‰.

Both the measured and age-corrected values of $^{206}Pb/^{204}Pb$, $^{207}Pb/^{204}Pb$, and $^{208}Pb/^{204}Pb$ for all analyzed samples, are shown in Table 4. Fifteen of the sulfide grains separated from the ores in the

Table 2
Oxygen, hydrogen, and carbon isotope data for quartz from the Yangshan gold belt (‰). Temperatures are from Li et al. (2007).

No.	Sample no.	Deposit	Paragenetic stage	$\delta^{18}O_{quartz}$ (‰)	Average $\delta^{18}O_{quartz}$ (‰)	δD (‰)	Average δD (‰)	T (°C)	$\delta^{18}O_{water}$ (‰)	Average $\delta^{18}O_{water}$ (‰)	$\delta^{18}C$ (‰)	Average $\delta^{18}C$ (‰)
1	YS-GL-05	Anba	Syn-metamorphic	18.5		−79		300	11.6		−4.0	
2	YS-PZB-04	Getiaowan	Early ore	17.0	16.5	−67	−72	295	9.9	9.4	−3.8	
3	YS-GTW-06	Getiaowan	Early ore	15.9		−77		295	8.8		–	
4	YS-GL-06	Anba	Main ore	19.3	19.3	−71	−70	235	9.6	9.6	−3.6	−3.4
5	YS-GL-07	Anba	Main ore	19.2		−68		235	9.5		−3.8	
6	YS-GL-02	Anba	Main ore	17.6		–		235	7.9		–	
7	YS-GYB-GL-07	Gaoloushan	Main ore	21.0		−78		235	11.3		−3.7	
8	YQ-1	Getiaowan	Main ore	18.5		−70		235	8.8		−3.6	
9	YS-PZB-02	Getiaowan	Main ore	18.8		−63		235	9.1		−3.4	
10	YS-PZB-7	Getiaowan	Main ore	18.3		−61		235	8.6		−3.7	
11	YS-PZB-09	Getiaowan	Main ore	18.1		−61		235	8.4		–	
12	YS-PZB-14	Getiaowan	Main ore	19.5		−71		235	9.8		−2.5	
13	YS-NS-TC-5	Nishan	Main ore	20.0		−78		235	10.3		–	
14	YS-NS-TC-6	Nishan	Main ore	21.5		−74		235	11.8		−2.6	
15	YS-AB-02	Anba	Late ore	19.7	19.7	−82	−73	195	7.7	7.7	−3.9	−3.5
16	YS-AB-03	Anba	Late ore	21.1		−81		195	9.1		−3.3	
17	YS-PZB-10	Getiaowan	Late ore	18.4		−56		195	6.4		−3.6	

"–" no analyzed data. The $\delta^{18}O_{water}$ values were calculated using equations for quartz-water provided by Zheng (1993).

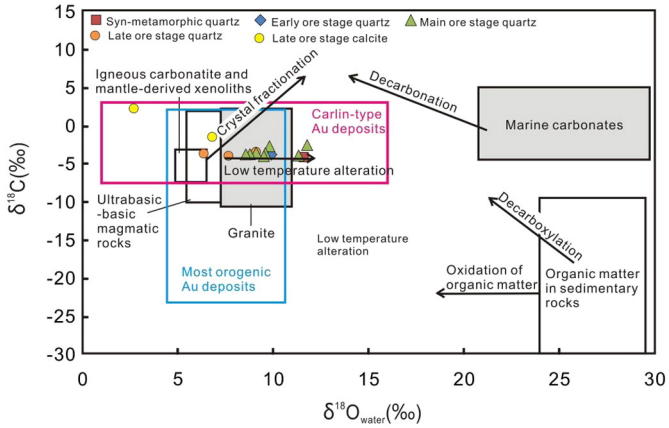

Fig. 6. The $\delta^{13}C_{CO2}$ and calculated $\delta^{18}O_{H2O}$ values of fluids at Yangshan. References for the fields of major carbon reservoirs and other deposits are from Liu et al. (1998). Data of two late ore-stage calcite are from Li et al. (2008).

Anba and Nishan gold deposits have $^{206}Pb/^{204}Pb$ ratios from 18.037 to 18.533, $^{207}Pb/^{204}Pb$ ratios from 15.554 to 15.686, and $^{208}Pb/^{204}Pb$ ratios from 38.195 to 39.020. Ores in the Yangshan gold belt have variable Pb isotopic compositions. The granitic dike-hosted ores have $^{206}Pb/^{204}Pb$ ratios from 18.162 to 18.980, $^{207}Pb/^{204}Pb$ ratios from 15.557 to 15.640, and $^{208}Pb/^{204}Pb$ ratios from 38.245 to 38.942. The Pb isotopic compositions of the Bikou Group are relatively variable compared with those of the granitic dike-hosted ores, and partially overlap those from the granitic dike-hosted ores and phyllite-hosted ores. Phyllite-hosted ores have higher $^{206}Pb/^{204}Pb$, $^{207}Pb/^{204}Pb$, and $^{208}Pb/^{204}Pb$ ratios than the granitic dike-hosted ores. Using the U, Th, and Pb abundances of the wall-rock sample and the 208 Ma mineralization age of Li (2013a), the age-corrected Pb isotopic compositions of whole rocks were calculated (Table 4, Fig. 8). The age-corrected Pb isotopic ratios for the ores and the Bikou Group—$^{206}Pb/^{204}Pb$ ratios, 17.350 to 20.163; $^{207}Pb/^{204}Pb$ ratios, 15.456 to 15.907; and $^{208}Pb/^{204}Pb$ ratios, 37.759 to 41.642—are lower than the measured values of Pb isotopic ratios (Table 4, Fig. 8).

5.3. Sr isotope composition of sulfides and fluids

To supplement the Sr isotope data from sulfides, the isotope values of pyritohedron pyrite and arsenopyrite in porphyry granitic dikes given in Zhang et al. (2009) are included in Table 5: the $(^{87}Sr/^{86}Sr)_i$ values of pyrite in Devonian metasedimentary rocks in that paper are excluded because of the coexistence of syn-metamorphic pyrite and hydrothermal pyrite. Using the ore-formation age of 208 Ma (Li, 2013a), the age-corrected $(^{87}Sr/^{86}Sr)_i$ values of pyrite are 0.70627 to 0.71304, and those of arsenopyrite are 0.71258 to 0.71294. Age-corrected Devonian metasedimentary rocks have the highest $(^{87}Sr/^{86}Sr)_i$ values from 0.71367 to 0.71882 (Liu et al., 2008), whereas the $(^{87}Sr/^{86}Sr)_i$ values of granitic dikes in our study are 0.70865 to 0.71395; the Bikou Group has the lowest $(^{87}Sr/^{86}Sr)_i$ values from 0.70343 to 0.71006 (Yan et al., 2004; Li et al., 2007) (Table 5, Fig. 9).

6. Discussion

6.1. Sources of ore-forming fluids and metals

6.1.1. Source of ore fluids

The $\delta^{18}O$ values of quartz (15.9‰–21.5‰) and the calculated $\delta^{18}O_{H2O}$ values of ore-forming fluids (6.4‰–11.8‰) from the Yangshan

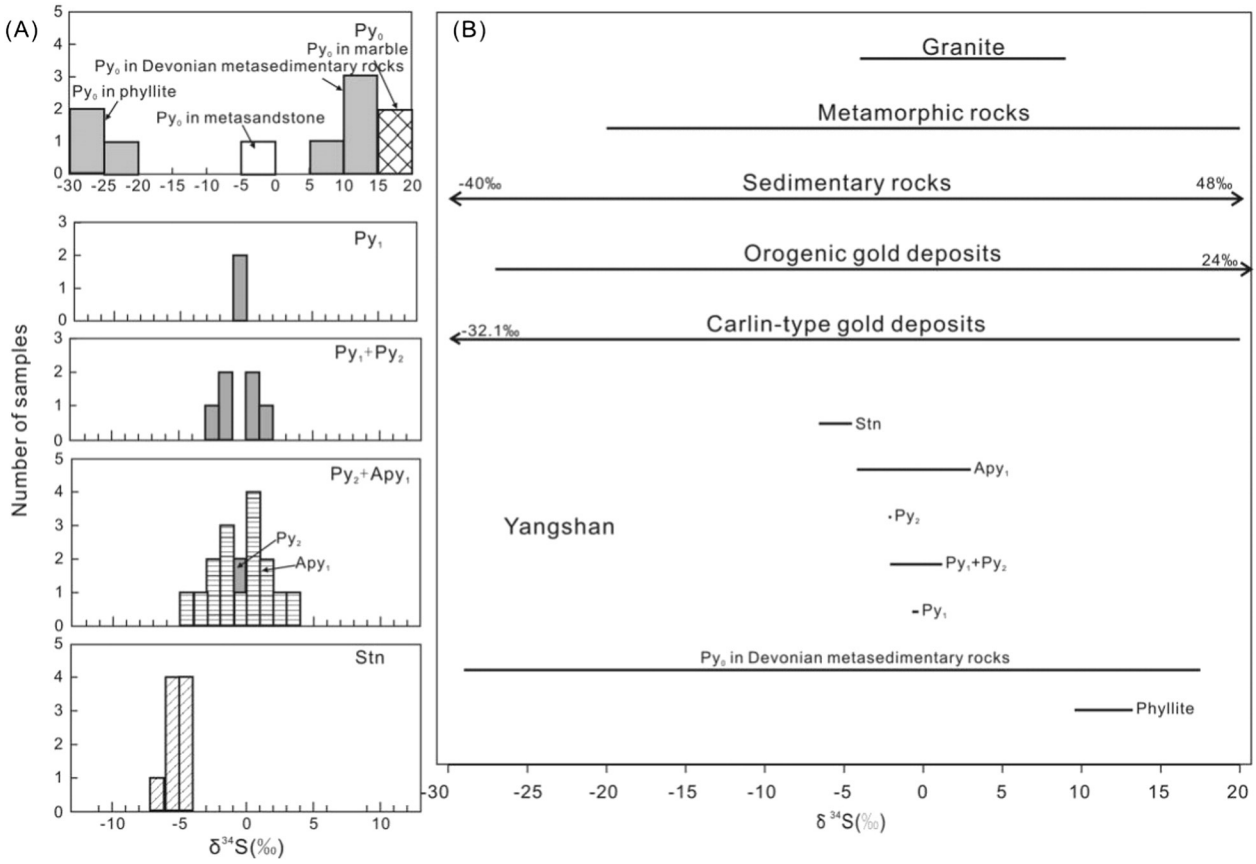

Fig. 7. (a) Histograms of $\delta^{34}S$ values of syn-metamorphic and hydrothermal pyrite from the Yangshan gold belt. (b) Comparison of sulfur isotope compositions of four mineralization stages at Yangshan. The ranges of major sulfur reservoirs and other deposits are given in the text.

Table 3
Sulfur isotope data for sulfides from gold deposits of the Yangshan gold belt.

No.	Sample no.	Host rock	Paragenetic stage	$\delta^{34}S$ (‰)	Average	Reference
1	AB10PD4-103-a	Phyllite-hosted ore	Py_0	7.6		This study
2	AB10PD4-103-b	Phyllite-hosted ore	Py_0	12.5		
3	YS-NS-10-06	Metasandstone-hosted ore	Py_0	−4.2		
4	YS-AB-10-HC-05-a	Granite dike-hosted ore	Py_1	−0.3	−0.6	
5	YS-AB-10-HC-05-b	Granite dike-hosted ore	Py_1	−0.7		
6	SM1-3	Granite dike-hosted ore	$Py_1 + Py_2$	0.7		
7	YS-AB-10-NC-05	Plagioclase granite porphyry-hosted ore	$Py_1 + Py_2$	−1.7		
8	YS-AB-10-PD1-01	Plagioclase granite dike-hosted ore	$Py_1 + Py_2$	−1.6		
9	YS-AB-10-PD1-04	Plagioclase granite porphyry-hosted ore	$Py_1 + Py_2$	−2.1		
10	YS-AB-10-PD2-02-a	Plagioclase granite porphyry-hosted ore	$Py_1 + Py_2$	0.8		
11	YS-AB-10-PD2-02-b	Plagioclase granite porphyry-hosted ore	$Py_1 + Py_2$	1.2		
12	AB10PD4-108(2)	Granite porphyry-hosted ore	Py_2	−2.1		
13	AB10PD4-101	Phyllite-hosted ore	Apy_1	−4.2	−0.5	
14	AB10PD4-102	Granite porphyry-hosted ore	Apy_1	−1.4		
15	AB10PD4-114	Phyllite-hosted ore	Apy_1	3.0		
16	AB10PD4-115	Phyllite-hosted ore	Apy_1	2.0		
17	YS-AB-10-PD2-02	Plagioclase granite porphyry-hosted ore	Apy_1	1.4		
18	YS-AB-10-PD4-21	Biotite plagioclase granite porphyry	Apy_1	0.6		
19	YS-ZK1709-10-03	Phyllite-hosted ore	Apy_1	−3.7		
20	SM1-2	Granite porphyry-hosted ore	Apy_1	0.0		
21	SM2-1	Phyllite-hosted ore	Apy_1	0.1		
22	SM2-3	Phyllite-hosted ore	Apy_1	−0.7		
23	SM2-4	Biotite granite porphyry-hosted ore	Apy_1	0.1		
24	SM2-6	Phyllite-hosted ore	Apy_1	−2.5		
25	AB10PD4-108(2)	Granite porphyry-hosted ore	Apy_1	−1.3		
26	AB10PD4-113	Granite porphyry-hosted ore	Apy_1	−1.7		
27	AB10PD4-116	Biotite granite porphyry-hosted ore	Apy_1	−0.5		
28	YS-AB-10-PD4-16	Plagioclase granite porphyry-hosted ore	Apy_1	1.5		
29	AB10PD4-108 (1)	Auriferous quartz vein in phyllite	Stn	−4.7	−5.3	
30	YS-AB-10-1haodong-01	Auriferous quartz vein in phyllite	Stn	−5.7		
31	YS-AB-10-4haodong-01	Auriferous quartz vein in phyllite	Stn	−4.5		
32	YS-AB-10-NC-05	Auriferous quartz vein	Stn	−5.4		
33	YS-AB-10-PD1-01	Auriferous quartz-calcite vein	Stn	−5.8		
34	YS-AB-10-PD1-05	Auriferous quartz-calcite vein	Stn	−6.6		
35	SM2-2	Auriferous quartz-calcite vein	Stn	−5.8		
36	SM4-1	Auriferous quartz-calcite vein	Stn	−4.8		
37	AB10PD4-118	Auriferous quartz vein	Stn	−4.8		
38	Y-31	Phyllite	Py_0	−24.6		Yang (2006)
39	Y-32	Phyllite	Py_0	−25.5		
40	Y-33	Phyllite	Py_0	−29.0		
41	Y-PD112BYY	Marble	Py_0	15.3		
42	Y-GLBYY	Marble	Py_0	17.5		
43	LJ-6	Phyllite	Py_0	10.9		Luo et al. (2004)
44	PDG-21	Phyllite	Py_0	10.1		Yan et al. (2010)

gold belt are consistent with those of vein quartz from orogenic gold provinces worldwide (10–22‰ for $\delta^{18}O_{quartz}$ values and 5–15‰ for $\delta^{18}O_{H2O}$ values: Clayton et al., 1972; Böhlke and Kistler, 1986; Kyser et al., 1986; Kerrich, 1987; Golding et al., 1989; Goldfarb et al., 1991, 1997; McCuaig and Kerrich, 1998; Kerrich et al., 2000; Jia et al., 2001, 2003). The calculated $\delta^{18}O_{H2O}$ values of the Yangshan gold belt increase slightly from the early to main ore stages (9.4‰ → 9.7‰), indicating either fluid–rock interaction with $\delta^{18}O$-rich wall rocks (22.4‰ for fresh phyllite: Yang, 2006), or input of $\delta^{18}O$-rich fluid from an external source. The latter is less likely because the petrology, Th and salinities of fluid inclusions from the Yangshan gold deposits show little evidence of fluid mixing (Li et al., 2007). In addition, the extensive silicification, sericitization, sulfidation, and carbonatization surrounding orebodies in the Yangshan gold deposits (Li et al., 2014) show that fluid–rock interaction is a more probable model.

The δD_{H2O} values of fluid inclusions in the quartz range from −82‰ to −56‰ (Table 2), which are within the δD range of most orogenic gold deposits (Fig. 5; −81‰ to −5‰; Kerrich, 1987; McCuaig and Kerrich, 1998; Ridley and Diamond, 2000). The average δD values show little variability from early to late ore stage (−72‰ → −70‰ → −73‰). Yang (2006) suggested that the low $\delta^{18}O$ values account for the $\delta^{18}O$-depleted meteoric water mixing with the hydrothermal system during the late ore stage in the Yangshan gold belt. However, the nearly constant $\delta^{18}O_{quartz}$ and δD values of ore fluids for both the main and late ore stages are relatively high, indicating that meteoric water mixing during the late ore stage was unlikely. The decrease in the calculated $\delta^{18}O_{H2O}$ values from the main to late ore stage may be simply due to the decrease in temperature.

Most of the calculated $\delta^{18}O_{H2O}$ and measured δD data from the Yangshan gold belt fall in or near the metamorphic water and magmatic water fields (Fig. 5). However, the δD_{H2O} values of fluid inclusions in the quartz are obtained from many generations of fluid inclusions, typically with significant amounts being unrelated to the original mineral precipitation (Goldfarb and Groves, 2015). Previous studies have shown that the δD values of alteration minerals such as sericite and muscovite, are about 20–40‰ lighter than those of fluid inclusions in the quartz (Ojala et al., 1995; Yang et al., 2016a). Thus, we suggest that the calculated $\delta^{18}O_{H2O}$ and δD compositions of the ore fluids should fall in the metamorphic water area, which is consistent with the epizonal orogenic gold deposits in the Jiaodong Peninsula (Fan et al., 2003; Hu et al., 2006; Yang et al., 2009, 2015c, 2016a,b; Wang et al., 2015), similar to most orogenic gold deposits, and far removed from the Carlin-type gold deposits (Arehart, 1996; Hofstra et al., 2000; Emsbo et al., 2003; Lubben et al., 2012; Fig. 5). The $\delta^{13}C_{CO2}$ values (−4‰ to −2.5‰, average −3.5‰; Table 2) of fluid inclusions in the different stages of quartz from the gold deposits in the Yangshan gold belt are similar, and are higher than those of carbon reservoirs such as continental crust (−7‰; Faure, 1986), mantle carbon (−5‰; Hoefs, 2004), and organic

Table 4
Lead isotope ratios for sulfides and host rocks from the Yangshan gold belt.

Sample type	Sample no.	Paragenetic stage	$^{208}Pb/^{204}Pb^a$	$^{207}Pb/^{204}Pb^a$	$^{206}Pb/^{204}Pb^a$	$^{208}Pb/^{204}Pb^b$	$^{207}Pb/^{204}Pb^b$	$^{206}Pb/^{204}Pb^b$	References
Granite porphyry-hosted ore	AB10PZB-1		38.454	15.576	18.808	37.963	15.543	18.154	This study
Granite porphyry-hosted ore	AB10PZB-2		38.294	15.564	18.469	38.096	15.551	18.221	
Granite-hosted ore	AB10PZB-4		38.309	15.567	18.162	38.130	15.550	17.831	
Granite-hosted ore	AB10PZB-5		38.644	15.638	18.498	38.428	15.621	18.148	
Granite porphyry-hosted ore	AB10PZB-6		38.245	15.557	18.179	38.125	15.539	17.810	
Plagioclase granite porphyry-hosted ore	ZK363-2		38.428	15.583	18.236	38.159	15.561	17.804	
Granite porphyry-hosted ore	AB10PD1W-1		38.942	15.640	18.980	38.454	15.602	18.226	
Granite-hosted ore	AB10PD1W-2		38.363	15.558	18.244	38.107	15.537	17.821	
Plagioclase granite porphyry-hosted ore	YS-AB-10-PD2-02		38.290	15.563	18.241	38.097	15.535	17.680	
Granite porphyry-hosted ore	AB10PD4-108(2)		38.385	15.579	18.584	38.180	15.548	17.986	
Biotite plagioclase granite porphyry-hosted ore	YS-AB-10-PD4-18		38.281	15.566	18.193	38.120	15.546	17.791	
Biotite plagioclase granite porphyry-hosted ore	YS-AB-10-PD4-21		38.341	15.572	18.359	38.113	15.541	17.747	
Phyllite-hosted ore	GTW10GD-1		39.545	15.713	18.817	38.805	15.686	18.285	
Phyllite-hosted ore	GTW10GD-4		40.156	15.742	19.253	39.229	15.712	18.653	
Phyllite-hosted ore	ZK1716-1		39.602	15.682	18.943	38.949	15.660	18.515	
Phyllite-hosted ore	ZK1716-2		40.291	15.744	19.252	39.106	15.709	18.564	
Phyllite-hosted ore	YS-AB-10-PD4-12		39.855	15.738	19.019	39.152	15.718	18.621	
Phyllite-hosted ore	AB10PD4-104		39.346	15.719	18.702	38.991	15.705	18.428	
Phyllite-hosted ore	AB10PD4-107		42.751	15.848	20.924	41.642	15.809	20.163	
Phyllite-hosted ore	YS-AB-10-PD4-03		40.395	15.746	19.261	39.297	15.714	18.616	
Pyrite	AB10PD4-103	Py_1	38.611	15.684	18.182	–	–	–	
Pyrite	AB10PD4-108(2)	Py_2	38.264	15.566	18.100	–	–	–	
Pyrite	SM1-3	$Py_1 + Py_2$	38.195	15.554	18.037	–	–	–	
Pyrite	SM2-4	$Py_1 + Py_2$	38.242	15.569	18.160	–	–	–	
Pyrite	YS-AB-10-PD2-02	$Py_1 + Py_2$	38.258	15.561	18.224	–	–	–	
Pyrite	YS-AB-10-PD4-17	$Py_1 + Py_2$	38.752	15.680	18.227	–	–	–	
Pyrite	YS-NS-10-04	$Py_1 + Py_2$	38.577	15.614	18.225	–	–	–	
Pyrite	YS-NS-10-05	Py_3	38.296	15.574	18.087	–	–	–	
Arsenopyrite	AB10PD4-113	Apy_2	38.246	15.562	18.048	–	–	–	
Arsenopyrite	AB10PD4-114	$Apy_2 + Apy_3$	39.015	15.686	18.489	–	–	–	
Arsenopyrite	AB10PD4-115	Apy_2	38.962	15.680	18.417	–	–	–	
Arsenopyrite	SM1-2	Apy_2	38.280	15.574	18.423	–	–	–	
Arsenopyrite	SM2-3	$Apy_2 + Apy_3$	38.900	15.686	18.349	–	–	–	
Arsenopyrite	SM2-4	Apy_2	38.234	15.568	18.115	–	–	–	
Arsenopyrite	SM4-2	$Apy_2 + Apy_3$	39.020	15.681	18.533	–	–	–	
Arsenopyrite	YS-AB-10-PD4-16	Apy_2	38.294	15.571	18.305	–	–	–	
Bikou Group (meta-basalt)			38.999	15.597	18.438	38.688	15.582	18.137	Zhang et al. (2002a,b)
Bikou Group (meta-basalt)			40.069	15.928	18.763	39.566	15.907	18.347	Li et al. (2007)
Bikou Group (meta-basalt)			39.157	15.833	18.017	38.929	15.820	17.763	
Bikou Group (meta-basalt)			38.945	15.814	17.91	38.803	15.806	17.755	
Bikou Group (phyllite)			38.128	15.471	17.644	37.824	15.456	17.350	Zhou (1991)
Bikou Group (phyllite)			38.064	15.553	18.016	37.759	15.538	17.720	
Bikou Group (siltstone)			38.394	15.552	18.126	38.087	15.537	17.829	

"–" no data available.
[a] Measured values.
[b] Age-corrected values at 208 Ma.

matter in sedimentary rocks (−30 to −10‰; Faure, 1986), whereas they are lower than the values of marine carbonate (0‰; Faure, 1986; Zheng and Chen, 2000). Those values are generally within the range of most orogenic gold deposits (Fig. 6; −23‰ to 2‰; Rye and Rye, 1974; Kerrich, 1987; Kontak and Kerrich, 1997; McCuaig and Kerrich, 1998; Ridley and Diamond, 2000), and also within the range of Carlin-type gold deposits (Fig. 6; −7.5‰ to 3.1‰; Ilchik, 1990; Hofstra et al., 2000; Emsbo et al., 2003). The $\delta^{13}C_{CO2}$–$\delta^{18}O_{H2O}$ values and the trend from the syn-metamorphic stage to the late ore stage, show that the fluids could be derived mostly from marine carbonate and partly from granitic rocks in the Yangshan gold belt (Fig. 6).

The isotopic data from the ore-stage sulfide minerals can be used to shed light on the source of the fluids associated with the pyrite and the gold event. The Sr isotopic compositions of sulfides and the wall rocks (Table 5; Fig. 9) show that the strontium in the ore fluid could have come from the granitic dikes and rocks of the Bikou Group, which is in agreement with the tectonic interpretation developed by Liu et al. (2008).

6.1.2. Source of metals

The $\delta^{34}S$ values of hydrothermal pyrite, arsenopyrite, and stibnite range from −6.6‰ to 3‰ (Table 3), and some of the values are lower than the minimum $\delta^{34}S$ value of granitic rocks, but within the $\delta^{34}S$ value ranges of metamorphic and sedimentary rocks, and also within the range of orogenic gold deposits (Fig. 7; −27.2‰ to 24‰; Goldfarb et al., 1997, 2004; McCuaig and Kerrich, 1998; Salier et al., 2005; Chang et al., 2008; Chen et al., 2012; Ding et al., 2014) and Carlin-type gold deposits (Fig. 7; −32.1‰ to 20‰; Arehart, 1996; Hofstra et al., 2000; Emsbo et al., 2003; Kesler et al., 2005). The wide range of values for syn-metamorphic pyrite in the gold deposits of the Yangshan gold belt is similar to those in sedimentary rocks (Fig. 7). In addition, the syn-metamorphic pyrite in marble has similar $\delta^{34}S$ values (15. 3–17. 5‰; Table 3) to those of contemporaneous seawater (Holser,

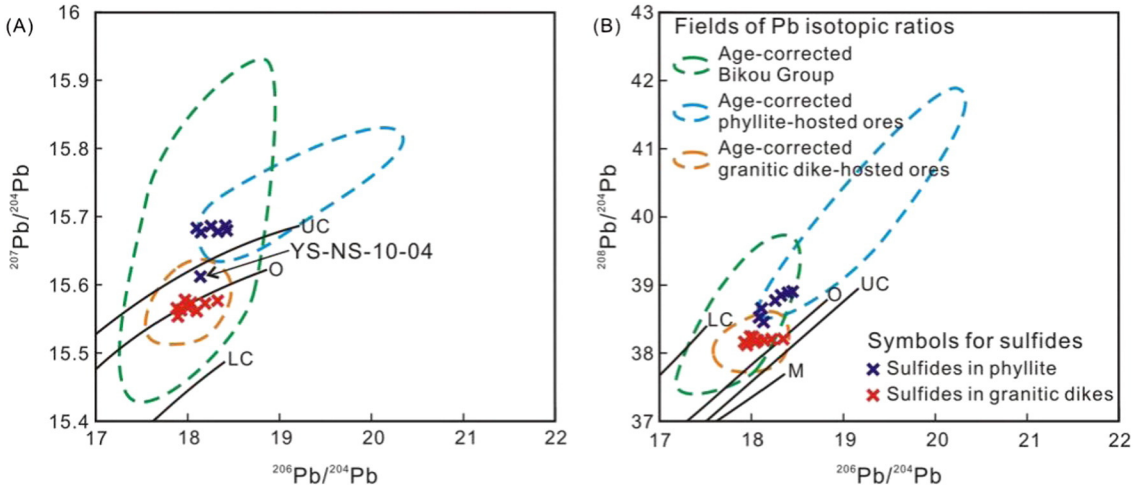

Fig. 8. Plots of (a) $^{207}Pb/^{204}Pb$ vs $^{206}Pb/^{204}Pb$ and (b) $^{207}Pb/^{204}Pb$ vs $^{206}Pb/^{204}Pb$, showing the lead isotopic compositions of sulfides and host rocks in the Yangshan gold belt. The evolution lines for the major geological units are from Zartman and Haines (1988).

1977), showing that the sulfur originated from sulfate ions in seawater (Yang, 2006). The $\delta^{34}S$ values of syn-metamorphic pyrite from the Devonian metasedimentary rocks (10.1–10.9‰) are within the range of the phyllite, indicating that the host strata are the sulfur source of the syn-metamorphic pyrite (Fig. 7). The narrow range of $\delta^{34}S$ values around zero for hydrothermal pyrite (−2.1 to 1.2‰; Table 3) and the unimodal distribution indicate that the sulfur in the gold deposits was derived from a uniform reservoir with a deep source (Faure, 1986).

Table 5
Rb–Sr isotope data from the gold deposits in the Yangshan gold belt.

Sample type	Sample no.	Rb	Sr	$^{87}Rb/^{86}Sr$	$^{87}Sr/^{86}Sr$	±2σ	$(^{87}Sr/^{86}Sr)_i$[a]	Reference
Granite porphyry	AB10PZB-1	163.3	87.5	5.411	0.729115	14	0.713109	This study
Granite porphyry	AB10PZB-2	161.3	96.0	4.873	0.727322	15	0.712908	
Granite	AB10PZB-4	104.4	202.0	1.497	0.713083	15	0.708655	
Plagioclase granite porphyry	ZK363-2	110.5	208.1	1.537	0.715110	14	0.710564	
Granite porphyry	AB10PDIW-1	168.9	57.2	8.573	0.739313	15	0.713954	
Granite	AB10PDIW-2	21.8	160.8	0.392	0.713298	15	0.712138	
Plagioclase granite porphyry	YS-AB-10-PD2-02	209.3	93.2	6.513	0.731570	10	0.712305	
Granite porphyry	AB10PD4-108(2)	180.1	105.2	4.962	0.727527	14	0.712850	
Biotite plagioclase granite porphyry	YS-AB-10-PD4-18	201.5	83.4	7.008	0.732736	11	0.712007	
Biotite plagioclase granite porphyry	YS-AB-10-PD4-21	209.0	113.1	5.355	0.727049	14	0.711209	
Siltstone	31	207.9	126.5	4.766	0.732920	–	0.718822	Liu et al. (2008)
Siltstone	32	146.9	115.7	3.681	0.727200	–	0.716312	
Siltstone	33	221.3	151.4	4.240	0.730830	–	0.718288	
Siltstone	39	42.7	209.0	0.592	0.715420	–	0.713669	
Granite porphyry	561	142.6	233.1	1.771	0.715080	–	0.709841	
Granite porphyry	4030	197.7	141.1	4.062	0.724670	–	0.712655	
Granite porphyry	PD1309	140.4	72.7	5.598	0.725650	–	0.709091	
Granite porphyry	4034	157.5	88.7	5.145	0.725580	–	0.710361	
Bikou Group (volcanic rocks)	1	–	–	0.092	0.704470	–	0.704198	Yan et al. (2004)
Bikou Group (volcanic rocks)	2	–	–	0.034	0.703530	–	0.703429	
Bikou Group (meta-basalt)	1	23.4	563.0	0.121	0.710420	–	0.710062	Li et al. (2007)
Bikou Group (meta-basalt)	2	0.2	111.0	0.006	0.707350	–	0.707332	
Bikou Group (meta-basalt)	3	0.1	143.0	0.003	0.706670	–	0.706661	
pyrite	461-1B-1	–	–	6.325	0.726740	–	0.708032	Zhang et al. (2009)
pyrite	461-1B-2	–	–	7.223	0.727640	–	0.706273	
pyrite	461-1B-3	–	–	4.363	0.721650	–	0.708745	
pyrite	461-1B-4	–	–	4.900	0.722730	–	0.708235	
pyrite	461-1B-5	–	–	5.824	0.725170	–	0.707944	
pyrite	461-1B-6	–	–	5.129	0.722550	–	0.707378	
pyrite	112-12-1	–	–	1.721	0.717410	–	0.712319	
pyrite	112-12-2	–	–	2.241	0.719670	–	0.713041	
pyrite	112-12-3	–	–	0.942	0.715760	–	0.712975	
pyrite	112-12-4	–	–	1.380	0.716490	–	0.712408	
pyrite	112-12-5	–	–	2.451	0.720020	–	0.712770	
pyrite	112-12-6	–	–	1.475	0.717190	–	0.712827	
Arsenopyrite	Jan-38	–	–	0.327	0.713890	–	0.712923	
Arsenopyrite	Feb-38	–	–	0.483	0.714120	–	0.712691	
Arsenopyrite	Mar-38	–	–	0.421	0.714190	–	0.712945	
Arsenopyrite	Apr-38	–	–	0.401	0.713970	–	0.712784	
Arsenopyrite	May-38	–	–	0.425	0.714190	–	0.712933	
Arsenopyrite	Jun-38	–	–	0.405	0.713780	–	0.712582	

"–" no data available.
[a] Calculated at 208 Ma.

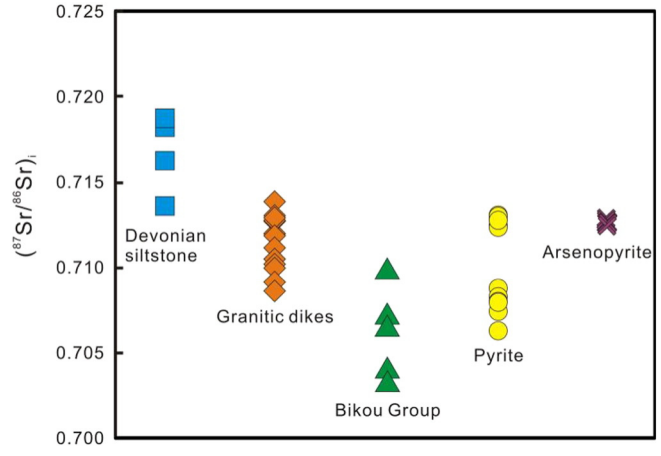

Fig. 9. Sr isotopic compositions of sulfides and host rocks at Yangshan.

Sulfide minerals usually contain very low concentrations of U and Th, and insignificant radiogenic Pb isotopes (Zhang, 1992; Zhang et al., 2000; Wu et al., 2002). Therefore, the Pb isotopes of sulfides from ore deposits are commonly used to constrain the source of the Pb (Browning et al., 1987; Tosdal et al., 2003; Goldfarb et al., 2004; Chen et al., 2012; Ayuso et al., 2013; Ding et al., 2014). For samples from the Yangshan gold belt, most of the Pb isotopic compositions of the ore-related pyrite and arsenopyrite fall within the range of the rocks of the Bikou Group. However, the Pb isotope values of sulfides (except for sample YS-NS-10-04; Fig. 8) overlap the field of their direct wall rocks. This suggests that the source of lead in the ore-related sulfides is their immediate host rocks regardless of the specific sulfide mineral and paragenetic stage. In contrast to other samples, the Pb isotope signature of pyrite from phyllite sample YS-NS-10-04 is within the field of granitic dikes, which may be due to its location at the contact zone between phyllite and granitic dike. Consequently, the Pb isotopic composition of Au-bearing sulfide minerals in the gold deposits of the Yangshan gold belt suggests that the host rocks contributed the lead to the formation of the sulfides, and therefore, by inference, could also have contributed some, if not all, of the gold. The average gold content of rocks of the Bikou Group and Devonian Sanhekou Group are 4.5 ppb and 4.6 ppb, respectively, which is higher than that of other rocks in the Qinling Orogen (Yuan et al., 2008).

6.2. Evolution of ore-forming fluids in the Yangshan gold belt

6.2.1. Syn-metamorphic stage

The peak of regional metamorphism in the Yangshan gold belt occurred earlier than 226 Ma (Li et al., 1999; Zhang et al., 2002b). The Devonian metasedimentary rocks were metamorphosed to greenschist facies with mineral assemblages of sericite + chlorite + quartz ± calcite (Dong, 2004). The H–O–C–S isotopic data in this study show that the syn-metamorphic stage fluids were derived from devolatilization of the Devonian metasedimentary rocks during the regional metamorphism (Figs 4-6; Tables 2, 3). This may have released abundant Au-related elements, such as As, Bi, Co, Cu, Mn, Ni, Pb, Sb, V, and Zn, as well as the gold now present at economic concentrations in the Yangshan gold belt (Li et al., 2014). However, the C–O–S–Sr isotopic data indicate that the Bikou Group and granitic dikes may also be part of the source reservoir for the ore-stage fluids, in addition to the Devonian metasedimentary rocks (Figs. 5, 6, 8).

6.2.2. Early ore stage

The ^{40}Ar–^{39}Ar ages for hydrothermal sericite show that the gold mineralization in the Yangshan gold belt is ca. 208 Ma (Li, 2013a), which is at least 20 million years younger than the peak of regional metamorphism of the West Qinling (Zhang et al., 1996) and about seven million years later than the emplacement of the granitoid dikes, which has been mineralized (Yang et al., 2015b). The ages, however, overlap the 216–200 Ma retrograde metamorphism of granulites in the Mianlue Suture Zone (Zhang et al., 2002b; Liang et al., 2013). The isotope data show that the early ore-stage fluids are similar to those of the syn-metamorphic stage (Figs 4-6; Tables 2, 3) and were derived mainly from the country rocks during their retrograde metamorphism at depth, which is consistent with the sulfide chemistry results (Li et al., 2014).

6.2.3. Main ore stage

In the main ore stage, sericitization and silicification are the dominant alteration types and are associated with sulfide precipitation and gold mineralization. Oxygen isotopic values indicate the widespread fluid interaction with $\delta^{18}O$-rich wall rocks during the main ore-forming event. This is also supported by the study of the sulfide geochemistry (Li et al., 2014).

6.2.4. Late ore stage

Consistent with the early and main ore stage fluids, the fluids in the late ore stage originated from metamorphic water and the Bikou Group, granitic dikes and Devonian metasedimentary rocks are the source reservoirs, based on the H–O–C–S–Sr isotopes. The high concentrations of arsenic and gold in Py_3 and Apy_3, as well as the stibnite and free gold observed in the late ore stage, indicate the release of Au from pyrite and/or arsenopyrite to form free gold, under slightly lower temperature and (or) pressure conditions than the main ore stage (Li et al., 2007; Li et al., 2014).

6.3. Ore genesis of the Yangshan gold belt

6.3.1. Comparison with other gold deposits in the Western Qinling

Based on previous studies, gold deposits in the Western Qinling orogenic belt can be divided into orogenic-type and Carlin-type gold deposits (Yun, 2005; Li, 2013b; Liu et al., 2010). The orogenic-type gold deposits, such as Maanqiao, Shuangwang, Baguamiao, and Manaoke, are hosted in the South Qinling Block and Mianlue Suture Zone, whereas the Carlin-type gold deposits, including Jinlongshan and Zhaishang, are situated near the boundary between the South Qinling Block and North Qinling Block (Fig. 1; Supplementary table 2).

The deposits in the Yangshan gold belt, together with other orogenic gold deposits in Western Qinling, are hosted in Devonian phyllite, slate and siltstone, with or without granitic dikes, which is consistent with typical orogenic gold deposits also commonly hosted in metamorphosed clastic rock terranes. The alteration surrounding these deposits is dominated by silicification, carbonatization, sulfidization, and sericitization. Their ore-forming temperatures range from 139 °C to 400 °C, and the metallogenic fluids originated from metamorphic or magmatic sources. Moreover, their calculated $\delta^{18}O_{H2O}$ values vary between 1.0 and 18.6‰, δD from −95 to −56‰, $\delta^{13}C$ from −17 to +0.9‰, and $\delta^{34}S$ values from −6.6 to +15.4‰ (Yun, 2005; Zhu et al., 2009; Li, 2013a).

In contrast, the Carlin-type deposits in West Qinling are mainly hosted in different Devonian metasedimentary rocks, mainly metasandstone and marble, and their dominant alteration type is decarbonatization. The ore-forming fluid for the Jinlongshan gold deposit was a mixed interlayer and meteoric water, and that for the Zhaishang gold deposit was meteoric water. Their ore-forming temperatures (120–268 °C) are slightly lower than those of the orogenic deposits in Western Qinling. Their calculated $\delta^{18}O_{H2O}$ values vary between 4.1 and 14.7‰, with much lower δD values ranging from −105 to −63‰, much higher $\delta^{13}C$ values ranging from −4.0 to 1.5‰, and $\delta^{34}S$ values ranging from −4.2 to 19.8‰ (Zhang et al., 2002a, 2014; Li, 2013b; Liu et al., 2010).

Overall, the geological characteristics and C–H–O–S isotopic signatures of the deposits in Yangshan gold belt are much more like those

Table 6
Summary of the critical characteristics of orogenic gold deposits, Carlin-type gold deposits, and gold deposits in the Yangshan gold belt. Modified from Groves et al. (2003), McCuaig and Kerrich (1998), Hofstra et al. (2000) and Goldfarb et al. (2005).

Critical characteristics	Orogenic gold deposits	Carlin type gold deposits	Yangshan gold belt
Tectonic setting	Deformed continental margin mainly of allochthonous terranes; compressional to transpressional regime	Back-arc extension and thinning of continental crust	Orogenic belt
Structural style	Ductile to brittle-ductile, reverse, strike-slip faults or oblique-slip; anticlinal domes	High angle fault, large anticline, the intersect of different faults	Fold and strike-slip faults
Host rock	Any type of rock	Mainly carbonate and clastic rocks	Altered clastic rocks and granitic dikes
Metamorphic grade of host rocks	Mainly greenschist facies but subgreenschist to lower granulite facies	No or weak metamorphism	Greenschist facies
Mineralization style	Veins, breccias, disseminated	Disseminated	Disseminated, veins
Alteration types	Carbonation, sericitization, sulfidation, silicification, albitization, tourmalinization	De-carbonation, intense silicification, illitization, kaolinization	Carbonation, sericitization, sulfidation, silicification
Ore mineral assemblages	Pyrite, arsenopyrite, stibnite	Pyrite, marcasite, arsenopyrite, realgar, orpiment, stibnite, cinnabar	Pyrite, arsenopyrite, stibnite
Temperature (°C)	220–600	160–250	195–295
Oxygen isotope (‰)	5–15	−19–18.6	6.4–11.8
Hydrogen isotope (‰)	−81 to −5	−170 to −40	−82 to −56
Carbon isotope (‰)	−23–2	−7.5–3.1	−4.0 to −2.5
Sulfur isotope (‰)	−27.2–24.0	−32.1–20.0	−6.6–3.0

of orogenic gold deposits and are distinct from Carlin-type gold deposits in Western Qinling (Supplementary table 2). Therefore, we suggest that the deposits in the Yangshan gold belt are orogenic type gold deposits.

6.3.2. Comparison of geological characteristics among different deposit types

The main characteristics of orogenic gold deposits, Carlin-type gold deposits, and the Yangshan gold belt are summarized in Table 6. The Yangshan gold belt was formed in the West Qinling orogenic belt and controlled by regional-scale strike-slip faults, which is similar to the tectonic setting and structural styles of orogenic gold deposits.

In summary, most of the geological characteristics of the Yangshan gold belt (tectonic setting, structural style, metamorphic grade of host rocks, alteration types, ore mineralogy), together with the H–O isotope data, are similar to those of orogenic gold deposits and distinct from Carlin-type gold deposits (Table 6). The several isotopic systems discussed in this paper indicate the important contribution of the Devonian metasedimentary rocks to the fluids and metals in the gold belt deposits. Further, they demonstrate the validity of the orogenic gold model for classification of the gold deposits of the Yangshan gold belt.

7. Conclusions

(1) The H–O isotope composition of quartz in the gold deposits in the Yangshan gold belt show that the ore-forming fluids are mainly metamorphic fluids that formed from devolatilization of the Devonian metasedimentary rocks during regional metamorphism. This is similar to other orogenic gold deposits and different from the Carlin-type gold deposits. The C–O–S–Sr isotope data for minerals and host rocks indicate that the Bikou Group and granitic dikes also contributed fluids and metals to the hydrothermal system.
(2) The isotopic data for the early ore-stage fluids are similar to those for the syn-metamorphic stage and were mainly derived from the country rocks during their prograde metamorphism. Oxygen isotope compositions indicate widespread fluid interaction with $\delta^{18}O$-rich wall rocks during the main ore stage in the Yangshan gold belt.
(3) Comparison of the geological and isotopic characteristics of the deposits in Yangshan gold belt, orogenic gold deposits, and Carlin-type gold deposits, indicates that the Yangshan gold deposits are orogenic gold deposits.

Supplementary data to this article can be found online at http://dx.doi.org/10.1016/j.gexplo.2016.06.006.

Acknowledgments

We thank Richard Goldfarb of the China University of Geosciences, for his comments and suggestions, which helped to greatly improve the manuscript, and Cayce A Gulbransen of USGS for assistance with the sulfur isotope experiment, and Tony Cockbain for his assistance with English. This work was financially supported by the National Basic Research Program of China (Grant Nos. 2015CB452605 and 2009CB421008), the Public Welfare Scientific Research Funding of China (Grant No. 201411048), the 111 Project under the Ministry of Education and the State Administration of Foreign Experts Affairs, China (Grant No. B07011), the Fundamental Research Funds for the Central Universities (No. 2-9-2014-055), and the Geological Investigation Work Project of the China Geological Survey (Grant No. 1212011121090).

References

Yan, Q.R., Andrew, D.H., Wang, Z.Q., Yan, Z., Peter, A.D., Wang, T., Liu, D.Y., Song, B., Jiang, C.F., 2004. Geochemistry and tectonic setting of the Bikou volcanic terrane on the northern margin of the Yangtze plate. Acta Petrol. Mineral. 23, 1–11.
Arehart, G.B., 1996. Characteristics and origin of sediment-hosted disseminated gold deposits: a review. Ore Geol. Rev. 11, 383–403.
Ayuso, R.A., Kelley, K.D., Eppinger, R.G., Forni, F., 2013. Pb–Sr–Nd isotopes in surficial materials at the pebble porphyry Cu–Au–Mo deposit, southwestern Alaska: can the mineralizing fingerprint be detected through cover? Econ. Geol. 108, 543–562.
Browning, P., Groves, D.I., Blockley, J.G., Rosman, A.K.J., 1987. Lead isotope constraints on the age and source of gold mineralization in the Archean Yilgarn Block, Western Australia. Econ. Geol. 82, 971–986.
Chang, Z.S., Large, R.R., Maslennikov, V., 2008. Sulfur isotopes in sediment-hosted orogenic gold deposits: evidence for an early timing and a seawater sulfur source. Geology 36, 971–974.
Chen, H.Y., Chen, Y.J., Baker, M.J., 2012. Evolution of ore-forming fluids in the Sawayaerdun gold deposit in the Southwestern Chinese Tianshan metallogenic belt. J. Asian Earth Sci. 49, 131–144.
Clayton, R.N., O'Neil, J.R., Mayeda, T.K., 1972. Oxygen isotope exchange between quartz and water. J. Geophys. 77, 3057–3067.
Deng, J., Wang, Q.F., Wan, L., Liu, H., Yang, L.Q., Zhang, J., 2011. A multifractal analysis of mineralization characteristics of the Dayingezhuang disseminated-veinlet gold deposit in the Jiaodong gold province of China. Ore Geol. Rev. 40, 54–64.

Deng, J., Liu, X.F., Wang, Q.F., Pan, R.G., 2014a. Origin of the Jiaodong-type Xinli gold deposit, Jiaodong Peninsula, China: constraints from fluid inclusion and C–D–O–S–Sr isotope compositions. Ore Geol. Rev. 65, 674–686.
Deng, J., Wang, Q.F., Li, G.J., Santosh, M., 2014b. Cenozoic tectono-magmatic and metallogenic processes in the Sanjiang region, southwestern China. Earth-Sci. Rev. 138, 268–299.
Ding, Q.F., Wu, C.Z., Santosh, M., Fu, Y., Dong, L.H., Qu, X., Gu, L.X., 2014. H–O, S and Pb isotope geochemistry of the Awanda gold deposit in southern Tianshan, Central Asian orogenic belt: implications for fluid regime and metallogeny. Ore Geol. Rev. 62, 40–53.
Dong, H., 2004. Disintegration of the 'Sanhekou Group' of the Sanhekou area, southern Qinling and its age. J. Stratigr. 28, 59–63 (in Chinese with English abstract).
Dong, Y., Zhang, G.W., Neubauer, F., Liu, X.M., Genser, J., 2011. Tectonic evolution of the Qinling orogen, China: review and synthesis. J. Asian Earth Sci. 81, 213–237.
Dong, Y.P., Zhang, X.N., Liu, X.M., Li, W., Chen, Q., Zhang, G.W., Zhng, H.F., Yang, Z., Sun, S.S., Zhang, F.F., 2014. Propagation tectonics and multiple accretionary processes of the Qinling Orogen. J. Asian Earth Sci. 84, 84–98.
Du, Z.T., Wu, G.G., 1998. Study on Tectonic Systems and Gold Metallogenic Tectonic-Dynamics in the Region of West Qinling. Geological Publishing House, Beijing (in Chinese with English abstract).
Emsbo, P., Hofstra, A.H., Lauha, E.A., Griffin, G.L., Hutchinson, R.W., 2003. Origin of high-grade gold ore, source of ore fluid components, and genesis of the Meikle and neighboring Carlin-type deposits, Northern Carlin Trend, Nevada. Econ. Geol. 98, 1069–1105.
Fan, H.R., Zhai, M.G., Xie, Y.H., Yang, J.H., 2003. Ore-forming fluids associated with granite-hosted gold mineralization at the Sanshandao deposit, Jiaodong gold province, China. Mineral. Deposita 38 (6), 739–750.
Faure, G., 1986. Principles of Isotope Geology. 2nd edition. John Wiley and Sons, New York, pp. 1–1779.
Feng, J.Z., Wang, D.B., Wang, X.M., Shao, S.C., Ma, Z.G., Zhang, X.G., 2003. Geology and metallogenesis of the Baguamiao giant gold deposit in Fengxian, Shanxi province. Acta Geol. Sin. 77, 387–398 (in Chinese with English abstract).
Fu, S.H., Wang, P., 2000. Study of fluid inclusions and the constraint for ore-forming conditions of gold deposit at Manaoke, north-western Sichuan province. Acta Petrol. Sin. 16, 569–574 (in Chinese with English abstract).
Giesemann, A., Jäger, H.J., Norman, A.L., Krouse, H.R., Brand, W.A., 1994. Online sulfur-isotope determination using an elemental analyzer coupled to a mass spectrometer. Anal. Chem. 66, 2816–2819.
Goldfarb, R.J., Groves, D.I., 2015. Orogenic gold: common or evolving fluid and metal sources through time. Lithos 233, 2–26.
Goldfarb, R.J., Newberry, R.J., Pickthorn, W.J., Gent, C.A., 1991. Oxygen, hydrogen, and sulfur isotope studies in the Juneau Gold Belt, southeastern Alaska: constraints on the origin of hydrothermal fluids. Econ. Geol. 86, 66–80.
Goldfarb, R.J., Miller, L.D., Leach, D.L., Snee, L.W., 1997. Gold deposits in metamorphic rocks of Alaska. Econ. Geol. Monogr. 9, 151–190.
Goldfarb, R.J., Ayuso, R., Miller, M., Ebert, S.W., Marsh, E.E., Petsel, S.A., Miller, L.D., Bradley, D., Johnson, C., Johnson, C., McClelland, W., 2004. The Late Cretaceous Donlin Creek gold deposit, Southwestern Alaska: controls on epizonal ore formation. Econ. Geol. 99, 643–671.
Goldfarb, R.J., Baker, T., Dube, B., Groves, D.I., Hart, C.J.R., Gosselin, P., 2005. Distribution, character and genesis of gold deposits in metamorphic terranes. Economic Geology 100th Anniversary Volume. Society of Economic Geologists, Littleton, pp. 407–450.
Goldfarb, R.J., Taylor, R.D., Collins, G.S., Goryachev, N.A., Orlandini, O.F., 2014. Phanerozoic continental growth and gold metallogeny of Asia. Gondwana Res. 48–102.
Golding, S.D., McNaughton, N.J., Barley, M.E., Groves, D.I., Ho, S.E., Rock, N.M.S., Turner, J.V., 1989. Archean carbon and oxygen reservoirs: their significance for fluid sources and circulation paths for Archean mesothermal gold deposits of the Norseman–Wiluna belt, Western Australia. Econ. Geol. Monogr. 6, 376–388.
Groves, D.I., Goldfarb, R.J., Robert, F., Hart, C.J.R., 2003. Gold deposits in metamorphic belts: overview of current understanding, outstanding problems, future research, and exploration significance. Econ. Geol. 9, 1–29.
He, X.X., Zhu, X.K., Yang, C., Tang, S.H., 2005. High-precision analysis of Pb isotope ratios using MC-ICP-MS. Acta Geosci. Sin. 26, 19–22.
Hoefs, J., 2004. Stable Isotope Geochemistry. 5th revised and updated ed. Springer Verlag, Berlin, pp. 1–244.
Hofstra, A.H., Cline, J.S., Hagemann, S.G., Brown, P.E., Boulder, C.O., 2000. Characteristics and models for Carlin-type gold deposits. Reviews in Economic Geology 13. Society of Economic Geologists, pp. 163–220.
Holser, W.T., 1977. Catastrophic chemical events in the history of the ocean. Nature 267, 403–408.
Hu, F.F., Fan, H.R., Zhai, M.G., Jin, C.W., 2006. Fluid evolution in the Rushan lode gold deposit of Jiaodong Peninsula, eastern China. J. Geochem. Explor. 89 (1), 161–164.
Ilchik, R.P., 1990. Geology and geochemistry of the Vantage gold deposits, Alligator Ridge-Bald Mountain mining district, Nevada. Econ. Geol. Bull. Soc. Econ. Geol. 85, 50–75.
Jia, Y., Li, X., Kerrich, R., 2001. Stable isotope (O, H, S, C and N) systematics of quartz vein systems in the tubidite-hosted Central and North Deborah gold deposits of the Bendigo gold field, Central Victoria, Australia: constraints on the origin of oreforming fluids. Econ. Geol. 96, 705–721.
Jia, Y., Kerrich, R., Goldfarb, R., 2003. Metamorphic origin of ore-forming fluids for orogenic gold-bearing quartz vein systems in the North American Cordillera: constraints from a reconnaissance study of $\delta^{15}N$, δD, and $\delta^{18}O$. Econ. Geol. 98, 109–123.
Kerrich, R., 1987. The stable isotope geochemistry of Au–Ag vein deposits in metamorphic rocks. In: Kyser, T.K. (Ed.), Stable Isotope Geochemistry of Low Temperature Fluids 13. Mineralogical Association of Canada Short Course, pp. 287–336.
Kerrich, R., Goldfarb, R., Groves, D.I., Garwin, S., Jia, Y.F., 2000. The characteristics, origins, and geodynamic settings of supergiant gold metallogenic provinces. 43. Sci. China. Ser. D, pp. 1–68 (Suppl.).
Kesler, S.E., Riciputi, L.C., Ye, Z.J., Nevada, U.S.A., 2005. Evidence for a magmatic origin for Carlin-type gold deposits: isotopic composition of sulfur in the Betze-Post-Screamer deposit. Mineral. Deposita 40, 127–136.
Böhlke, J.K., Kistler, R.W., 1986. Rb-Sr, K-Ar, and stable isotope evidence for the ages and sources of fluid components of gold-bearing quartz veins in the Northern Sierra Nevada Foothills metamorphic belt, California. Econ. Geol. 81, 296–322.
Kontak, D.J., Kerrich, R., 1997. An isotopic (C, O, Sr) study of vein gold deposits in the Meguma terrane, Nova Scotia: implications for source reservoirs. Econ. Geol. 92, 161–180.
Kyser, T.K., Janser, B.W., Wilson, M.R., Hattie, I., 1986. Stable isotope geochemistry related to gold mineralization and exploration in the Western Shield. In: Clark, L.A. (Ed.), Gold in the Western Shield: CIM Special. 38, pp. 470–498.
Large, R.R., Bull, S.W., Maslennikov, V.V., 2011. A carbonaceous sedimentary source-rock model for Carlin-type and orogenic gold deposits. Econ. Geol. 106, 331–358.
Lei, S.B., 2011. Tectonic and Magmatic Constraints on Mineralization and Gold Prospecting of Yangshan Gold Belt, Gansu Province (PhD thesis) School of the Earth Sciences and Resources, China University of Geosciences, Beijing, pp. 1–126 (in Chinese with English summary).
Li, N., 2013a. Geochemistry of Ore-forming Processes in the Yangshan Gold Belt, West Qinling, Central China (PhD thesis) School of the Earth Sciences and Resources, China University of Geosciences, Beijing, pp. 1–147 (in Chinese with English summary).
Li, T., 2013b. Metallogenic Characteristics and Genesis of Au–Hg–Sb Ore Deposits in Jinlongshan District in Zhen'an, Shanxi (Master's thesis in Chang'an University) pp. 1–86 (in Chinese with English summary).
Li, J.Y., Wang, Z.Q., Zhao, M., 1999. ^{40}Ar–^{39}Ar thermochronological constraints on the timing of collisional orogeny in the Mian-Lue collision belt, southern Qinling Mountains. Acta Geol. Sin. 73, 208–215.
Li, J., Chen, Y.J., Li, Q.Z., Lai, Y., Yang, R.S., Mao, S.D., 2007. Fluid inclusion geochemistry and genetic type of the Yangshan gold deposit, Gansu, China. Acta Petrol. Sin. 23, 2144–2154 (in Chinese with English abstract).
Li, J., Chen, Y.J., Li, Q.Z., Mao, S.D., Qin, Y., Guo, J.H., Nan, Z.L., Yang, R.S., 2008. The C–H–O isotope systematics of the Yangshan gold deposit, Gansu and its implication for the ore-fluid origin. Acta Petrol. Sin. 24, 817–826.
Li, N., Yang, L.Q., Zhang, C., Zhang, J., Lei, S.B., Wang, H.T., Wang, H.W., Gao, X., 2012. Yangshan gold belt, West Qinling: constraints on ore-forming environment and material source. Acta Petrol. Sin. 28, 1577–1587.
Li, N., Deng, J., Yang, L.Q., Goldfarb, R., Zhang, C., Marsh, E., Lei, S.B., Koenig, A., Lowers, H., 2014. Paragenesis and geochemistry of ore minerals in the epizonal gold deposits of the Yangshan gold belt, West Qinling, China. Mineral. Deposita 49, 427–449.
Liang, S., Liu, L., Zhang, C.L., Yang, Y.C., Yang, W.Q., Kang, L., Cao, Y.T., 2013. Metamorphism and zircon U–Pb age of high-pressure mafic granulites in Mian–Lue suture zone, South Qinling orogen. Acta Petrol. Sin. 29, 1657–1674 (in Chinese with English abstract).
Liu, J.M., Liu, J.J., Zheng, M.H., Gu, X.X., 1998. Stable isotope compositions of micro-disseminated gold and genetic discussion. Geochimica 27, 585–591.
Liu, H.J., Chen, Y.J., Mao, S.D., Zhao, C.H., Yang, R.S., 2008. Element and Sr–Nb–Pb isotope geochemistry of granite-porphyry dykes in the Yangshan gold belt, western Qinling orogen. Acta Petrol. Sin. 24, 1101–1111 (in Chinese with English abstract).
Liu, J.J., Mao, G.J., Wu, S.H., Wang, J.P., Ma, X.H., Li, L.X., Liu, G.Z., Liao, Y.F., Zheng, W.J., 2010. Matallogenic characteristics and formation machanism of Zhaishang gold deposit, southern Gansu province. Mineral Deposits 29, 85–100 (in Chinese with English abstract).
Liu, C.H., Liu, J.J., Carranza, E.J.M., Yang, L.B., Wang, J.P., Zhai, D.G., Wang, Y.H., Wu, J., Dai, H.Z., 2015. Geological and geochemical constraints on the genesis of the Huachanggou gold deposit, western Qinling region, central China. Ore Geol. Rev. http://dx.doi.org/10.1016/j.oregeorev.2015.08.002.
Lubben, J.D., Cline, J.S., Barker, S.L.L., 2012. Ore fluid properties and sources from quartz-associated gold at the Betze-Post Carlin-type gold deposit, Nevada, United States. Econ. Geol. 107, 1351–1385.
Luo, X.M., Qi, J.Z., Yuan, S.S., Li, Z.H., 2004. Geological and microelement geochemical study of Yangshan gold deposit, Gansu Province. Geoscience 18, 203–209 (in Chinese with English abstract).
Mattauer, M., Matte, P., Malavieille, J., Tapponnier, P., Maluski, H., Qin, X.Z., Lun, L.Y., Qin, T.Y., 1985. Tectonics of the Qinling belt: build-up and evolution of eastern Asia. Nature 496–500.
McCuaig, T.C., Kerrich, R., 1998. P–T–t–deformation–fluid characteristics of lode gold deposits: evidence from alteration systematics. Ore Geol. Rev. 12, 381–453.
Meng, Q.R., Zhang, G.W., 1999. Timing of collision of the North and South China blocks: controversy and reconciliation. Geology 27, 123.
Meng, Q.R., Zhang, G.W., 2000. Geologic framework and tectonic evolution of the Qinling orogen, central China. Tectonophysics 323, 183–196.
Ojala, V.J., Groves, D.I., Ridley, J.R., 1995. Hydrogen isotope fractionation factors between hydrous minerals and ore fluids at low temperatures: evidence from the Granny Smith gold deposit, Western Australia. Mineral Deposits 30, 328–331.
Pei, X.Z., Zhang, G.W., Lai, S.C., Li, Y., Chen, L., Gao, M., 2002. Main geological features of the Mian–Lue tectonic belt on the southern margin of the West Qinling. Geol. Bull. China 21, 486–494 (in Chinese with English abstract).
Phillips, G.N., Powell, R., 2009. Formation of gold deposits: review and evaluation of the continuum model. Earth Sci. Rev. 94, 1–21.
Qi, J.Z., Yuan, S.S., Li, L., Fan, Y.X., Liu, W., Gao, Q.B., Sun, B., Guo, J.H., Li, Z.H., 2003. Geological and geochemical studies of Yangshan gold deposit, Gansu Province. Mineral Deposits 49, 24–31 (in Chinese with English abstract).
Qi, J.Z., Li, L., Yuan, S.S., Liu, Z.J., Liu, D.Y., Wang, Y.B., Li, Z.H., 2005. A SHRIMP U–Pb chronological study of zircons from quartz veins of Yangshan gold deposit, Gansu Province. Mineral Deposits 24, 141–150 (in Chinese with English abstract).

Qin, J.F., Lai, S.C., Li, Y.F., 2008. Slab break-off model for the Triassic post-collision adakitic granitoids in the Qinling orogenic belt, central China: zircon U–Pb ages, geochemistry and Sr–Nd–Pb isotopic constraints. Int. Geol. Rev. 50, 1080–1104.
Ridley, J.R., Diamond, L.W., 2000. Fluid chemistry of orogenic lode gold deposits and implications for genetic models. In: Hagemann, S.G., Brown, P.E. (Eds.), Gold in 2000: Reviews in Economic Geology. Vol. 13, pp. 141–162.
Rye, D.M., Rye, R.O., 1974. Homestake gold mine, South Dakota: I. Stable isotope studies. Econ. Geol. 69, 293–317.
Salier, B.P., Groves, D.I., McNaughton, N.J., Fletcher, I.R., 2005. Geochronological and stable isotope evidence for widespread orogenic gold mineralization from a deep-seated fluid source at ca 2.65 Ga in the Laverton gold province, Western Australia. Econ. Geol. 100, 1363–1388.
Sun, W.D., Li, S.G., Chen, Y.D., 2000. Zircon U–Pb dating of granitoids from south Qinling, Central China and their geological significance. Geochimica 29, 209–216.
Sun, W.D., Li, S.G., Chen, Y.D., Li, Y.J., 2002. Timing of synorogenic granitoids in the South Qinling, Central China: constraints on the evolution of the Qinling-Dabie Orogenic Belt. J. Geol. 110, 457–468.
Taylor, B.E., 1987. Stable Isotope Geochemistry of Ore-forming Fluid: Mineralogical Association of Canada Short Course. 13 pp. 337–445.
Tomkins, A.G., 2013. On the source of orogenic gold. Geology 41, 1255–1256.
Tosdal, R.M., Cline, J.S., Fanning, C.M., Wooden, J.L., 2003. Lead in the Getchell-Turquoise Ridge Carlin-type gold deposits from the perspective of potential igneous and sedimentary rock sources in northern Nevada: implications for fluid and metal sources. Econ. Geol. 98, 1189–1211.
Wang, K.X., 2012. Geological and Geochemical Features and Genesis of the Shuangwang Gold Deposit in Taibai County, Shanxi Province (Master's thesis in China University of Geosciences, Beijing) pp. 1–80 (in Chinese with English abstract).
Wang, K.Y., Yao, S.Z., Lv, X.B., 2001. Geochemistry of ore-forming fluids of Manaoke gold deposit, north-western Sichuan province. Geochimica 30, 273–281 (in Chinese with English abstract).
Wang, Z.L., Yang, L.Q., Guo, L.N., Marsh, E., Wang, J.P., Liu, Y., Zhang, C., Li, R.H., Zhang, L., Zheng, X.L., Zhao, H., 2015. Fluid immiscibility and gold deposition in the Xincheng deposit, Jiaodong Peninsula, China: a fluid inclusion study. Ore Geol. Rev. 65, 701–717.
Wei, L.M., 2004. Matallogenic Environment and Prediction for Baguamiao Gold Deposit Type in Qinling Region, China (Doctoral thesis in Chengdu University of Technology) pp. 1–133 (in Chinese with English abstract).
Wen, C.M., 2006. Geological features and genesis for Au deposit in the Yangshan Au ore belt, Gansu. Acta Geol. Sichuan 26, 223–227 (in Chinese with English abstract).
Wu, K.X., Hu, R.Z., Bi, X.W., Peng, J.T., Tang, Q.L., 2002. Ore lead isotopes as a tracer for ore-forming material sources: a review. Geochimica 30, 74–80 (in Chinese with English abstract).
Xu, J.F., Castillo, P.R., Li, X.H., Yu, X.Y., Zhang, B.R., Han, Y.W., 2002. MORB-type rocks from the Paleo-Tethyan Mian–Lueyang northern ophiolite in the Qinling Mountains, central China: implications for the source of the low $^{206}Pb/^{204}Pb$ and high $^{143}Nd/^{144}Nd$ mantle component in the Indian Ocean. Earth Planet. Sci. Lett. 198, 323–337.
Yan, Q.R., Wang, Z.Q., Yan, Z., Hanson, A.D., Druschke, P.A., Liu, D.Y., Song, B., Jian, P., Wang, T., 2003. SHRIMP age and geochemistry of the Bikou volcanic terrane: implications for Neoproterozoic tectonics on the northern margin of the Yangtze craton. Acta Geol. Sin. 77, 479–490.
Yan, F.Z., Qi, J.Z., Guo, J.H., 2010. Geology and Exploration of Yangshan Gold Deposit in Gansu Province. Geological Publishing House, Beijing (in Chinese with English abstract).
Yang, R.S., 2006. Geology, Geochemistry and Genesis of Yangshan Gold Deposit, Gansu Province, China (Doctoral thesis in Peking University, Beijing) pp. 1–173.
Yang, T., 2012. Geological and Geochemical Constraints on the Genesis and Tectonic Setting of the Liziyuan Orogenic Gold Deposit in West Qinling Orogen (China. Master's thesis in Northwest University) pp. 1–90 (in Chinese with English abstract).
Yang, R.S., Chen, Y.J., Zhang, F.X., Li, Z.H., Mao, S.D., Liu, H.J., Zhao, C.H., 2006. Chemical Th–U–Pb ages of monazite from the Yangshan gold deposit, Gansu province and their geologic and metallogenic implications. Acta Petrol. Sin. 22, 2603–2610 (in Chinese with English abstract).
Yang, G.C., Qi, J.Z., Dong, H.F., Guo, J.H., Li, Z.H., 2007. Geology and isotope characters of Yangshan gold deposit, Gansu. Geophys. Prospect. 4, 37–41 (in Chinese with English abstract).
Yang, L.Q., Deng, J., Guo, C.Y., Zhang, J., Jiang, S.Q., Gao, B.F., Gong, Q.J., Wang, Q.F., 2009. Ore-forming fluid characteristics of the Dayingezhuang gold deposit, Jiaodong gold province, China. Resour. Geol. 59, 181–193.
Yang, L.Q., Deng, J., Qiu, K.F., Ji, X.Z., Santosh, M., Song, K.R., Song, Y.H., Geng, J.Z., Zhang, C., Hua, B., 2015a. Magma mixing and crust–mantle interaction in the Triassic monzogranites of Bikou Terrane, central China: constraints from petrology, geochemistry, and zircon U–Pb–Hf isotopic systematics. J. Asian Earth Sci. 98, 320–341.
Yang, L.Q., Deng, J., Dilek, Y., Qiu, K.F., Ji, X.Z., Taylor, R.D., Yu, J.Y., 2015b. Geochronology, and petrogenesis of the Late Triassic Puziba granitoid dikes in the Mianlue suture zone, Qinling orogen, China. Geol. Soc. Am. Bull. 127, 1831–1854.
Yang, L.Q., Deng, J., Guo, R.P., Guo, L.N., Wang, Z.L., Chen, B.H., Wang, X.D., 2015c. World-class Xincheng gold deposit: an example from the giant Jiaodong gold province. Geosci. Front. http://dx.doi.org/10.1016/j.gsf.2015.08.006.
Yang, L.Q., Deng, J., Guo, L.N., Wang, Z.L., Li, X.Z., Li, J.L., 2016a. Origin and evolution of ore fluid, and gold deposition processes at the giant Taishang gold deposit, Jiaodong Peninsula, eastern China. Ore Geol. Rev. 72, 585–602.
Yang, L.Q., Deng, J., Wang, Z.L., Guo, L.N., Li, R.H., Groves, D.I., Danyushevskiy, L., Zhang, C., Zheng, X.L., Zhao, H., 2016b. Relationships between gold and pyrite at the Xincheng gold deposit, Jiaodong Peninsula, China: implications for gold source and deposition in a brittle epizonal environment. Econ. Geol. 111, 105–126.
Yuan, S.S., Li, W.L., Zhang, Y., Chang, C.J., 2008. Metallogenic process and model of the super-large Yangshan gold deposits in Gansu province. Geol. Res. 17 (2), 92–101.
Yun, Z.W., 2005. Metallogenic Control Factor and Prediction for Maanqiao Gold Deposit, Shanxi Province (Master's thesis in Chang'an University) pp. 1–79 (in Chinese with English abstract).
Zartman, R.E., Haines, S.M., 1988. The plumbotectonic model for Pb isotopic systematics among major terrestrial reservoirs—a case study for bi-directional transport. Geochim. Cosmochim. Acta 52, 1327–1339.
Zhang, L.G., 1992. Present status and aspects of lead isotope geology. Geophys. Prospect. 28, 21–29 (in Chinese with English abstract).
Zhang, G.W., Meng, Q.R., Lai, S.C., 1995. Tectonics and structure of Qinling orogenic belt. Sci. China Ser. D 38, 1379–1394.
Zhang, G.W., Meng, Q.R., Yu, Z.P., Sun, Y., Zhou, D.W., Guo, A.L., 1996. Orogenesis and dynamics of the Qinling orogen. Sci. China Ser. D 39, 225–234.
Zhang, Q., Pan, J.Y., Shao, S.X., 2000. An interpretation of ore lead sources from lead isotopic compositions of some ore deposits in China. Geochimica 29, 232–238 (in Chinese with English abstract).
Zhang, G.W., Zhang, B.R., Yuan, X.C., Xiao, Q.H., 2001. Qinling Orogenic Belt and Continental Dynamics. Sci Press Beijing, pp. 1–806 (in Chinese with English abstract).
Zhang, J., Chen, Y.J., Zhang, F.X., Li, C., 2002a. Geochemical study of ore fluid in Jinlongshan Carlin-type gold ore belt in southwestern Shaanxi Province. Mineral Deposits 21, 283–291 (in Chinese with English abstract).
Zhang, Z.Q., Zhang, G.W., Tang, S.H., Xu, J.F., Yang, Y.C., Wang, J.H., 2002b. The age of Anzishan granulite, Qinling Mianlue suture zone. Chin. Sci. Bull. 47, 1751–1755.
Zhang, G.W., Dong, Y.P., Lai, S.C., Guo, A.L., Meng, Q.R., Liu, S.F., Cheng, S.Y., Yao, A.P., Zhang, Z.Q., Pei, X.Z., Li, S.Z., 2004. Mianlue tectonic zone and Mianlue suture zone on southern margin of Qinling–Dabie orogenic belt. Sci. China Ser. D 47, 300–316.
Zhang, L., Yang, R.S., Mao, S.D., Lu, Y.H., Qin, Y., Liu, H.J., 2009. Sr and Pb isotopic feature and ore-forming material source of the Yangshan gold deposit. Acta Petrol. Sin. 25, 2811–2822 (in Chinese with English abstract).
Zhang, J., Li, L., Gilbert, S., Liu, J.J., Shi, W.S., 2014. LA-ICP-MS and EPMA studies on the Fe–S–As minerals from the Jinlongshan gold deposit, Qinling Orogen, China: implications for ore-forming processes. Geol. J. 49, 482–500.
Zhao, G.C., Wilde, S.A., Cawood, P.A., Sun, M., 2001. Archean blocks and their boundaries in the North China Craton: lithological, geochemical, structural and P–T path constrains and tectonic evolution. Precambrian Res. 107, 45–73.
Zheng, Y.F., 1993. Calculation of oxygen isotope fractionation in hydroxyl-bearing silicates. Earth Planet. Sci. Lett. 120, 247–263.
Zheng, Y.F., Chen, J.F., 2000. Stable Isotope Geochemistry. Science Press, Beijing, pp. 1–316 (in Chinese with English abstract).
Zhou, L., 1991. Source beds of ore-forming metals and mechanism of Pb and Zn mobilization of Xicheng ore field. Gansu province. Earth Sci. 16, 199–206 (in Chinese with English abstract).
Zhu, L.M., Zhang, G.W., Lee, B., Guo, B., Gong, H.J., Kang, L., Lv, S.L., 2009. Zircon U–Pb dating and geochemical study of the Xianggou granite in the Ma'anqiao gold deposit and its relationship with gold mineralization. Sci. China Ser. D Earth Sci. 39, 700–720 (in Chinese with English abstract).